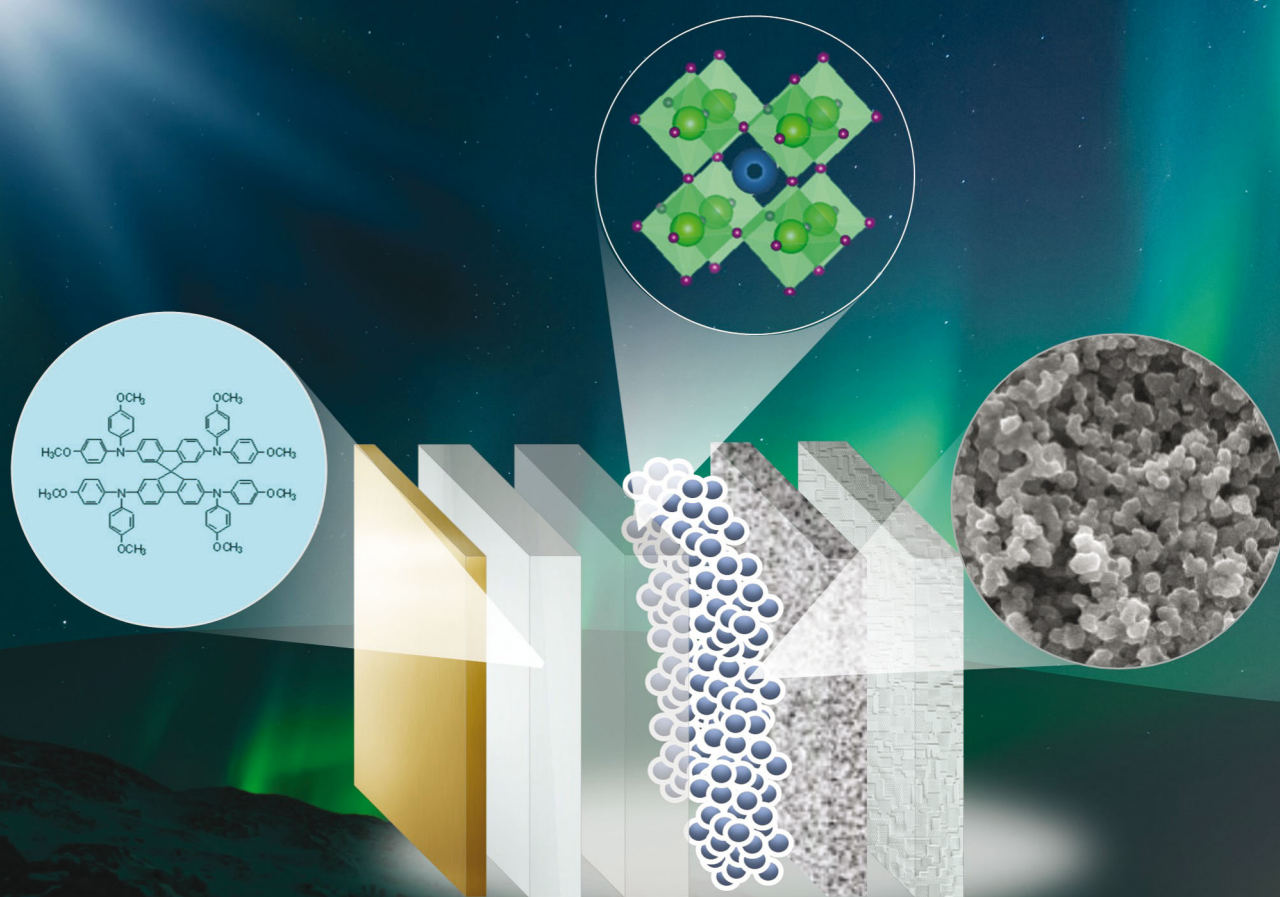


PCCP

Physical Chemistry Chemical Physics
www.rsc.org/pccp



Themed issue: Physical chemistry of hybrid perovskite solar cells

ISSN 1463-9076



PERSPECTIVE

Tingting Xu, Tingli Ma *et al.*

Strategic improvement of the long-term stability of perovskite materials and perovskite solar cells

175
YEARS



Cite this: *Phys. Chem. Chem. Phys.*,
2016, **18**, 27026

Strategic improvement of the long-term stability of perovskite materials and perovskite solar cells

Tingting Xu,^{*ab} Lixin Chen,^a Zhanhu Guo^c and Tingli Ma^{*b}

Perovskite solar cells (PSCs) have gained tremendous research interest in recent several years. To date the power conversion efficiency (PCE) of PSCs has been increased from 3.8% to over 22.1%, showing that they have a promising future as a renewable energy resource to compete with conventional silicon solar cells. However, a crucial challenge of PSCs currently is that perovskite materials and PSCs have limitations of easy degradation and inferior long-term stabilities, thus hampering their future commercial applications. In this review, the degradation mechanisms for instable perovskite materials and their corresponding solar cells are discussed. The stability study of perovskite materials and PSCs from the aspect of experimental tests and theoretical calculations is reviewed. The strategies for enhancing the stability of perovskite materials and PSCs are summarized from the viewpoints of perovskite material engineering, substituted organic and inorganic materials for hole transportation, alternative electrodes comprising mainly carbon and its relevant composites, interfacial modification, novel device structure construction and encapsulation, etc. Various approaches and outlooks on the future direction of perovskite materials and PSCs are highlighted. This review is expected to provide helpful insights for further enhancing the stability of perovskite materials and PSCs in this exciting field.

Received 29th June 2016,
Accepted 24th August 2016

DOI: 10.1039/c6cp04553g

www.rsc.org/pccp

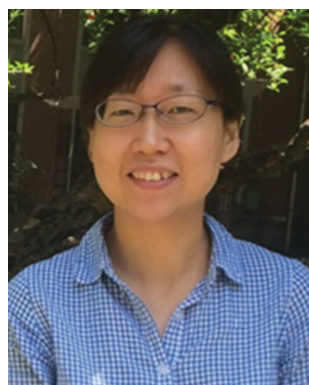
^a Department of Applied Chemistry, School of Science, Northwestern Polytechnical University, Xi'an, Shaanxi, 710129, P. R. China. E-mail: tingtingxu@nwpu.edu.cn

^b Graduate School of Life Science and Systems Engineering, Kyushu Institute of Technology, 2-4 Hibikino, Wakamatsu, Kitakyushu, Fukuoka 808-0196, Japan. E-mail: tinglima@life.kyutech.ac.jp

^c Integrated Composites Laboratory (ICL), Department of Chemical & Biomolecular Engineering, University of Tennessee, Knoxville, TN 37996, USA

1. Introduction

Photovoltaics (PVs) have been regarded as one of the most promising technologies to convert sunlight into electricity. PV technology typically includes inorganic types of solar cells such as silicon (Si), gallium arsenide (GaAs), copper indium gallium



Tingting Xu

Dr Tingting Xu is currently an associate professor in the Applied Chemistry Department at the School of Science, Northwestern Polytechnical University (NPU), Xi'an, P. R. China. She completed her PhD in Photovoltaics in the Electrical Engineering department at South Dakota State University (SDSU) in August 2012. She worked as a postdoctoral research associate at Kyushu Institute of Technology (KIT) in 2015–2016. She was awarded the Chinese Government Award for Outstanding Self-financed Students Abroad in 2011. Her research interests mainly focus on renewable energy including perovskite solar cells, dye/quantum dot sensitized solar cells and batteries.



Tingli Ma

Prof. Tingli Ma is a professor in the Graduate School of Life Science and Systems Engineering at Kyushu Institute of Technology (KIT) in Japan. From 2007 to the present, she has also worked at the State Key Laboratory of Fine Chemicals at Dalian University of Technology (DUT) in Dalian, P. R. China. She leads research teams studying dye-sensitized solar cells (DSSCs), perovskite solar cells (PSCs), and other renewable energy related projects including the development of solar catalysts, solar-powered hydrogen production, functional dyes and nanostructured semiconductor materials. She is also a council member of the following organizations: Japan Society for Chemistry; China Microfabrication Technology Council, China Instrument Society of Instrumentation, China Energy Society, China Solar Energy, and so on.

selenide (CIGS), *etc.*, and organic types of solar cells such as dye sensitized solar cells (DSSCs), quantum dot sensitized solar cells (QDSSCs), organic polymer solar cells (OPVs), *etc.* Particularly, organic solar cells with the advantages of low cost materials and simple solution-processing attract much research interest, leading to new directions for the next generation of PV technology.

Perovskite materials and their relevant solar cells have emerged as the rising-stars in the field of organic-inorganic hybrid solar cells since 2009.¹⁻⁴ Three-dimensional (3D) perovskite structured materials of methylammonium lead halide ($\text{CH}_3\text{NH}_3\text{PbX}_3$) ($X = \text{Cl}, \text{Br}, \text{I}$) or its mixed-halide crystal have been used as light harvesting materials in PSCs. Perovskite nanocrystals of metal halides have figure of merits of a direct bandgap, a large absorption coefficient, a high carrier mobility, long lifetime and ambipolar transport.⁵ The diffusion length of carriers (electrons and holes) for a mixed halide $\text{CH}_3\text{NH}_3\text{PbI}_{3-x}\text{Cl}_x$ is more than 1 μm , and for a triiodide $\text{CH}_3\text{NH}_3\text{PbI}_3$ is ~ 100 nm.⁶ In PSCs, the active layer of perovskite materials functions not only as a light absorber, but also as an excellent electron- and hole-transporting material. Due to their unique optical and electrical properties, PSCs have achieved an extraordinarily rapid growth over the last several years. The power conversion efficiency (PCE) of PSCs has been increased steadily from an initial value of 3.8% in 2009⁷ to a recent world-record high value of 22.1% as claimed by KRICT and UNIST.⁸ The PCE evolution of PSCs is shown as Fig. 1(a), and a roadmap of the main trend for the development of PSCs is shown in Fig. 1(b). The progress of PSCs has gone from using unstable liquid electrolytes to solid state hole-transporting materials (HTMs), and then moving to more concise morphology and composition control for forming uniform perovskite films, as well as interfacial engineering for minimizing charge recombination. The future trends of PSCs would focus on fabricating more robust and reliable devices for outdoor applications.

Currently, PSCs appear to exhibit outstanding photovoltaic performance and potential practical commercialization in the market. However, they are confronted with a serious long-term stability problem, mainly due to the unstable nature of perovskite materials in the environment and synergic factors of the functional components in PSCs. To the best of our knowledge, the most stable PSC reported in the literature underwent a test of 1440 h with a remaining PCE of 90%.⁹ While the stability testing conditions vary to a large extent in the PSC community, thus a characterization standard for the long-term stability testing in PSCs is imperative to guide the comparison of a device's duration performance. Meanwhile, with more and more research interest in the long-term stability problem of PSCs, degradation mechanisms for perovskite materials and their relevant solar cells are still far from maturity, and approaches to solve the instability of PSCs lag behind their fast growth of efficiency race. There are several reviews on the stability of perovskite materials and perovskite solar cells,¹⁰⁻¹³ in which most of the results on the long-term stability of PSCs were summarized. A review on the stability studies, especially on experimental tests and theoretical calculations for perovskite materials and PSCs, is rare; and a extensive review on the recent improvement of the long-term stability of PSCs, especially the most recent findings in this rapidly developing field, has not been fully discussed.

Hence, in this review, we focus on the stability study of perovskite materials and PSCs from perspectives of experimental characterization and theoretical calculations, and we also comprehensively evaluate and discuss the approaches aimed at enhancing the long-term stability of PSCs, including the engineering of perovskite materials, interfacial modification, new hole-transporting materials (HTLs), electrodes especially carbon based materials for counter electrodes (CEs), novel device configurations, device encapsulation, *etc.* The outlooks for enhancing the stability of PSCs are also included. This work gives insight on stability improvement in PSCs, leading to an understanding of how far we are from really stable PSCs.

2. Origin of the stability problem in perovskite solar cells

PSCs are generally fabricated by placing an electron-transporting layer (ETL) on conductive glass, and then subsequently depositing layers of a perovskite active layer, a hole-transporting layer (HTL), and an electrode. PSCs with architectures of (a) planar, (b) mesoporous, (c) inverted, (d) ETL free, (e) HTL free with a carbon electrode are shown in Fig. 2. The photovoltaic performance decay of PSCs is affected by unstable perovskite active layers, as well as the functional layers in which perovskite materials are incorporated. Here, the performance deterioration mechanism for PSCs is discussed according to the classification of different functional layers, *i.e.* perovskite layers, ETLs, HTLs, and electrodes. It would provide helpful insight to fully reveal the long-term stability problem of current PSCs.

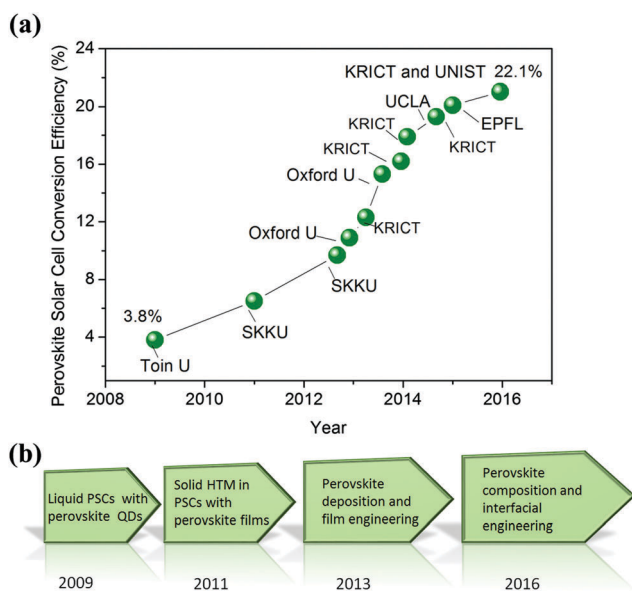


Fig. 1 (a) The power conversion efficiency (PCE) evolution of perovskite solar cells (PSCs) from 2009 to date; (b) main research trends in PSCs over the last several years.

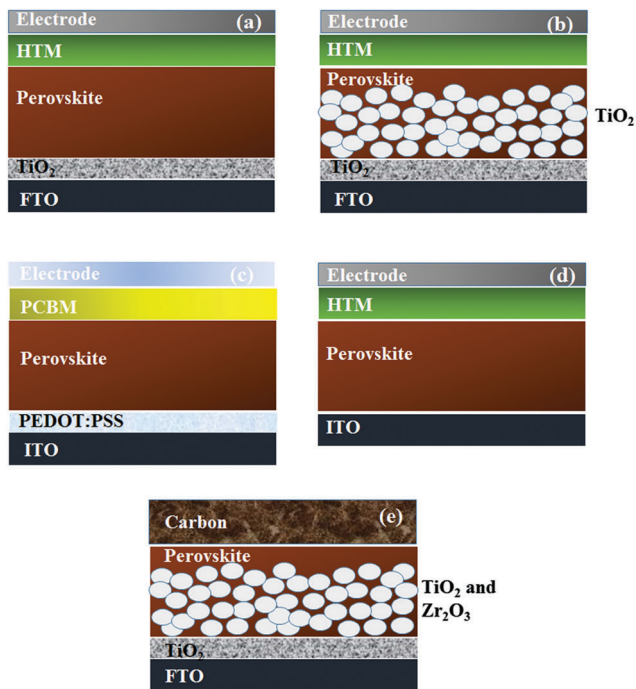


Fig. 2 Configurations of perovskite solar cells with (a) planar, (b) mesoporous, (c) inverted, (d) ETL free, and (e) HTL free with a carbon electrode.

2.1 Perovskite layers

Humidity is a major factor causing instability in perovskite materials. With a hygroscopic nature, perovskite materials such as $\text{CH}_3\text{NH}_3\text{PbI}_3$ readily react with water to finally decompose into $\text{CH}_3\text{NH}_3\text{I}$ and PbI_2 , involving intermediate byproducts of monohydrate $\text{MAPbI}_3 \cdot \text{H}_2\text{O}$ and dihydrate $(\text{MA})_4\text{PbI}_6 \cdot 2\text{H}_2\text{O}$ during the decomposition process.^{14–18} This is the general degradation mechanism triggered by moisture or water. On the other hand, the moisture content is critical for forming $\text{CH}_3\text{NH}_3\text{PbI}_3$ films with good morphology, a large grain size up to 500 nm, as well as decreased pinhole and grain boundaries,^{19–21} attributed to a so-called “moisture assisted crystal growth” phenomenon.²² The stability towards humidity in perovskite MAX_3 with mixed-halide atoms varies by tuning the composition of halide elements, for example $\text{MAPb}(\text{I}_{1-x}\text{Br}_x)_3$ is more stable when the Br content increases,²³ due to the smaller Br atom contributing a much more stable perovskite crystal structure than its I counterpart.^{23,24}

The thermal degradation of organic–inorganic perovskite materials takes place when the heating temperature increases,²⁵ and the color of the perovskite film changes from dark brown to yellow. A previous research study discovered that MAPbI_3 starts to decompose at a temperature of 230 °C, while the decomposition temperature for FAPbI_3 is 290 °C.²⁶ All-inorganic perovskites show better thermal stability due to the fact that the inorganic species are more stable compared with organic ones under thermal stress.

The photo-induced degradation of perovskites depends on the hybrid perovskite compositions of different substitutes in the crystal structures, and it is also related to the light intensity and environmental temperature.²⁷ UV light irradiation

combined with O_2 accelerates the degradation of perovskites via HI decomposition in iodide substituted perovskites.

A weak electrical bias initiates a rapid degradation of perovskite materials under humid conditions.^{28,29} Electrical stress induces ion migration and causes hysteresis effects of PSCs. Mobile ions, in particular methylammonium ions, drift along the electric field and build up certain stress regions within PSCs, leaving ion vacancies.²⁸ Leijtens *et al.* concluded that ion motion alone would not degrade PSCs, while combined factors of moisture, residual solvent and electric bias may damage devices and reduce their stability.¹⁰ The mechanism of electrical field induced PSC performance deterioration still needs more research to understand precisely how the applied bias affects the long-term stability of PSCs under working conditions.

Apart from lead perovskite materials, environmentally friendly Sn based perovskites have also been explored to fabricate lead-free perovskite solar cells.^{30–32} However, the stability study of lead-free perovskite materials is relatively scarcely reported. To sum up, perovskite materials are greatly affected by moisture/water associated decomposition. Factors such as thermal stress, oxygen, UV-light and solution processing, *etc.* all have severe effects on the stability of perovskites and PSCs.³³ Reports on perovskite degradation caused by thermal decomposition,^{27,34,35} crystal phase transition,^{36,37} photo-induced trap state formation³⁸ or photodecomposition, and electrically induced ion migration²⁹ provide helpful understanding of the instability problems of perovskites and PSCs.

2.2 Electron transporting layers (ETLs)

Metal oxide semiconductors such as TiO_2 , ZnO and SnO_2 have been applied as ETLs in PSCs to extract electrons from light absorbers.^{19,39–44} TiO_2 is the most extensively used ETL in PSCs adopted from a similar concept of dye sensitized solar cells (DSSCs). TiO_2 causes the PSCs to be instable because of its sensitive nature to UV-light. The mechanism of UV-induced TiO_2 degradation in PSCs remains under debate. One hypothesis was proposed by Snaith *et al.*,^{45,46} who ascribed the instability of PSCs to UV light-induced desorption of the surface absorbed O_2 on mesoporous TiO_2 films. Upon UV-light illumination on the TiO_2 surface, oxygen is desorbed owing to the recombination of holes in the valence band (VB) of TiO_2 with electrons at the oxygen adsorption sites,^{47,48} thus leaving free electrons in the conduction band (CB) of TiO_2 and positively charged empty oxygen vacancy sites. These free electrons would readily react with a p-type doped hole-transporting material (HTM) such as Spiro-OMeTAD, causing performance degradation of PSCs. Devices without TiO_2 materials presented a better stability of constant photocurrent performance for a continuous 1000 h of light exposure compared with those having TiO_2 ETLs.⁴⁵

Ito *et al.* explained the UV-light induced degradation mechanism of PSCs from a similar perspective to DSSCs.⁴⁹ They considered that the degradation of perovskite layers in PSCs may be due to the photocatalytic characteristics of TiO_2 . TiO_2 might extract electrons from the iodide anions (I^-) of perovskite materials under UV light exposure, and then the perovskite crystal structure may be destroyed

after releasing I_2 , causing performance deterioration of PSCs. However, since perovskites have different chemical properties from the redox electrolyte of I^-/I_3^- , the photocatalytic properties of TiO_2 need to be further studied to determine how UV-light intensity affects perovskite decomposition initiated by TiO_2 .

Some reports also pointed out that TiO_2 is critical for the long-term stability of PSCs.⁵⁰ Matsumoto *et al.* found that the photodecomposition of $CH_3NH_3PbI_3$ active films was degraded more slowly than the completed PSCs using TiO_2 ETLs.⁵¹ They regarded that interfaces within the specific device architecture would affect the degradation of PSCs. They also stated that the degradation of perovskite materials required light and moisture, and the degradation of PSCs became more severe under higher humidity, and had a linear relationship with the light intensity. The mechanism for UV-light degradation of PSCs still needs more research work to gain deep understanding.

2.3 Hole transporting materials (HTMs) and additives

For the majority of well-functioning PSCs, hole-transporting materials (HTMs) are essential to achieve a high PCE. So far, a mixed solution consisting of 2,2',7,7'-tetrakis(*N,N*-di-*p*-methoxyphenylamine)-9,9'-spirobifluorene (Spiro-OMeTAD) or its p-type form doped by dopants of Li-bis(trifluoromethanesulfonyl)imide (Li-TFSI) or Co-TFSI, and 4-*tert*-butylpyridine (TBP) additive is the most widely acknowledged HTM in PSCs. A previous research study revealed that a dopant was necessary for efficient charge transportation between Spiro-OMeTAD molecules, as π - π intermolecular stacking was lacking in the pristine Spiro-OMeTAD crystal structures.⁵² The Spiro-OMeTAD HTM is generally spin-coated on top of perovskite layers, while it has a great difficulty in obtaining a completely pin-hole free Spiro-OMeTAD HTM layer.⁵³ Thus species in the atmosphere can easily react with the Spiro-OMeTAD HTM and permeate from the tiny pinholes. Moisture and O_2 diffuse through these small pinholes to decompose the perovskite underneath the HTMs, meanwhile, mobile ions migrate from the perovskites to speed up the degradation of the HTMs. These degradation processes will lead to the aging of films and inferior cell performance in a short time. Qi *et al.* investigated the Spiro-OMeTAD HTM caused degradation of PSCs *via* a thermal deposition process,^{54,55} the doping effects of Li-bis(trifluoromethanesulfonyl)imide (Li-TFSI),⁵³ and the environmental effects of gas molecules (O_2 , $H_2O + N_2$, and N_2).⁵⁶ They discovered that Li-TFSI migrated from the bottom to the top across the Spiro-OMeTAD film when the solar cell was exposed to air. Li-TFSI gradually redistributed to the top surface of HTMs, inducing rapid film degradation and a decrease in the efficiency of PSCs. Besides, a spectrum-dependent mechanism for incident light induced oxidation of Spiro-OMeTAD with the LiTFSI dopant in PSCs was proposed by Meng *et al.*⁵⁷ They revealed that the oxidation of Spiro-OMeTAD could take place without perovskite's presence when the films were illuminated at a short wavelength range of 380 nm to 450 nm. In a wavelength range longer than 450 nm, Spiro-OMeTAD was only oxidized when the perovskite was involved in the oxidization reaction.

2.4 Electrodes

Metal electrodes are an important component in PSCs for charge collection. Commonly used metal electrodes in PSCs are gold, silver and aluminum (inverted structure). Silver is a cheaper choice compared to gold, but PSCs assembled with a silver electrode experience a fast degradation of the PCE. The reason for the degradation is that silver may react with perovskite materials and form silver chloride (AgCl) or silver iodide (AgI) under humid conditions, causing short circuits or shunting degradation of PSCs.⁵⁸ The migration of ions towards the electrode side and excess iodide accumulation at the interface of the perovskite/HTM/electrode were shown to be responsible for the degradation of PSCs.⁵⁹ The migration of methyl ammonium ions accelerated the formation of AgI *via* penetrating the small pinholes in Spiro-OMeTAD films.⁶⁰ Fig. 3 shows a hypothesis of perovskite film degradation at the interface of the metal cathode/HTM/perovskite proposed by Qi *et al.*⁶⁰ The initial step for PSC degradation takes place when water in ambient air diffuses from the pinholes of the Spiro-OMeTAD film as shown in Fig. 3(a). Then the perovskite film is decomposed into CH_3NH_3I , HI and PbI_2 (Fig. 3(b)). Volatile species of iodine compounds react with the top Ag electrode and generate AgI. Meanwhile, the moisture and reactant species in air further degrade the perovskite film, leading to a more serious performance decay as shown in Fig. 3(c). The migration of ions may be a reversible process. The metal corrosive reactions occurring at the interface of the HTM/electrode or inside the HTM when the thermally evaporated metal diffused into the HTM, are irreversible degradation processes, causing performance degradation of PSCs. Gold has a high corrosion resistance to iodine, but it could also be corroded under oxidative conditions.⁶¹ A previous research study found that the iodine/iodide redox couple can react with gold to form AuI_2^- and AuI_3 .⁶² Therefore, metal-iodide corrosion induced by charge accumulation at interfaces is an indispensable reason for the degradation of PSCs.

As well as the above discussed factors, issues such as solution and carrier gas during device fabrication may also

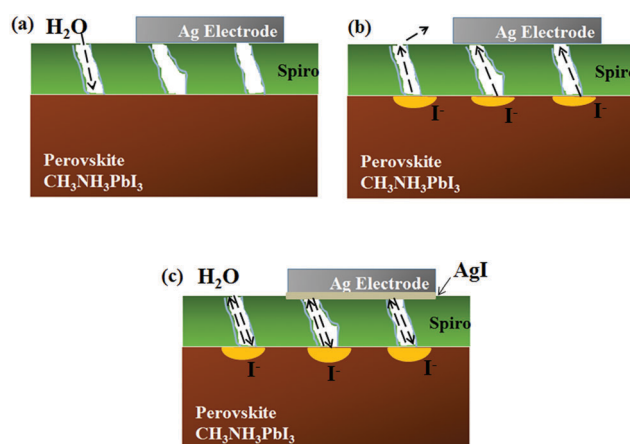


Fig. 3 Hypothesis of perovskite film degradation at the interface of metal cathode/Spiro-OMeTAD HTM/perovskite in a humid environment. Redrawn from ref. 60.

affect the stability of PSCs. The interfaces between each function layer are crucial for the stability of PSCs as well, where charge accumulation and recombination are likely to occur. In order to address these challenges and obtain stable PSCs, approaches to study the long-term stability of perovskite materials and PSCs are discussed in the next section. A variety of recent strategies targeting the stability improvement of PSCs are fully reviewed in our strategy section.

3. Experimental and theoretical methods to study the long-term stability of perovskite solar cells

After exploring a variety of degradation mechanisms for perovskite materials and PSCs, another critical question is how to monitor the degradation process of perovskites and PSCs qualitatively and quantitatively? Appropriate physical and chemical techniques are desired to study how environmental conditions affect perovskites and PSCs. Optical properties, crystal phase changes, crystallinities of bulk perovskite materials and their surface properties vary to a large extent during the decomposition processes. Other parameters including the carrier lifetime, mass loss, thermal and mechanical characteristics are valuable information to access the whole picture of the degradation of perovskite materials and the performance decay of PSCs as well. These parameters may provide some clues about avoiding a harsh environment or practicable caring for perovskite material preparation and device fabrication.

3.1 Experimental methods

Perovskite films decompose within a few days of exposure to air without effective encapsulation, and the film color changes from dark brown to yellow. Habisreutinger *et al.* stated that the color change of the lead halide may correlate with the bond dissociation and the transformation of the perovskite crystal structure, turning into a lower dimensional system after the methylamine cations reacted with water molecules.⁶³ We also

noticed that perovskite films of $\text{CH}_3\text{NH}_3\text{PbI}_3$ coated on glass decomposed completely in ambient air within a month.

UV-visible absorption spectroscopy is a commonly applied method to monitor the degradation process of perovskite materials. An obvious absorption decrease in the wavelength range of 530 nm to 800 nm can be observed from the absorption spectrum of perovskite films.⁶⁴ Fig. 4(a) shows the absorption changes of $\text{CH}_3\text{NH}_3\text{PbI}_3$ films kept at a relative 90% humidity in the dark at room temperature for different storage periods.¹⁷ The $\text{CH}_3\text{NH}_3\text{PbI}_3$ film had a sharp absorption decrease in the visible range from just prepared to that stored for 14 days, indicating a rapid decomposition of $\text{CH}_3\text{NH}_3\text{PbI}_3$ to PbI_2 . Kamat *et al.* studied the interaction between $\text{CH}_3\text{NH}_3\text{PbI}_3$ and H_2O vapor by evaluating the optical absorption properties of the perovskite in the ground-state and excited-states.¹⁷ The X-ray diffraction (XRD) spectrum supported the degradation of perovskite $\text{CH}_3\text{NH}_3\text{PbI}_3$ with the disappearance of the initial characteristic peaks of $\text{CH}_3\text{NH}_3\text{PbI}_3$ at 31.86° , 40.45° and 43.14° , assigned to the planes of (310), (224) and (314) for the tetragonal perovskite structure.^{64,65} New peaks of the decomposed product of PbI_2 were located at 34.3° (102), 39.5° (110), 52.4° (004), and for I_2 a peak was located at 38.7° (201).⁶⁴

In situ measurements are powerful techniques to study the degradation process of perovskite films from a dynamic perspective. Kelly *et al.* investigated the degradation mechanisms of $\text{CH}_3\text{NH}_3\text{PbI}_3$ films in a controlled humid environment *via in situ* absorption spectroscopy and *in situ* grazing incidence X-ray spectroscopy (GIXRD).¹⁸ Phase changes of the perovskite films during the degradation process were monitored. They found that the degradation of perovskites depended upon the humid conditions and the HTM layer coated on the top of perovskites. A hydrophobic HTM may be favorable for protecting the perovskites from moisture permeation. The same group also studied the thermal instability of $\text{CH}_3\text{NH}_3\text{PbI}_3$ films deposited on a ZnO surface through *in situ* GIXRD experiments and density functional theory (DFT) calculations.³⁵ A proton-transfer reaction was proposed to explain that the decomposition mechanism occurred at the interface of $\text{ZnO}/\text{CH}_3\text{NH}_3\text{PbI}_3$, considering the basic nature of ZnO. Fig. 4(b–e) shows the

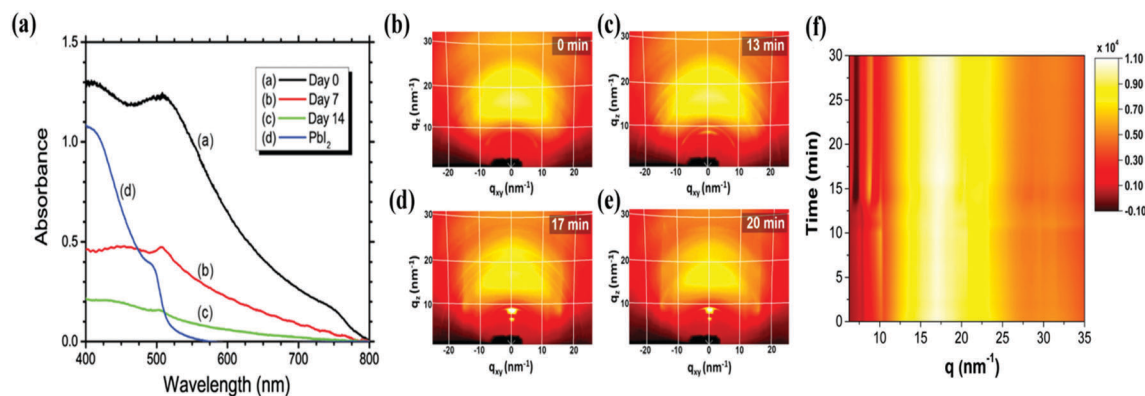


Fig. 4 (a) UV-visible absorption spectra of perovskite $\text{CH}_3\text{NH}_3\text{PbI}_3$ for varied time storages in 90% humidity in the dark at room temperature;¹⁷ 2D GIXRD patterns of $\text{SiO}_2/\text{ZnO}/\text{CH}_3\text{NH}_3\text{PbI}_3$ films after different heating times of 0 min (b), 13 min (c), 17 min (d), and 20 min (e) at 100°C in air;³⁵ (f) the azimuthally integrated intensity plot of the sample $\text{SiO}_2/\text{ZnO}/\text{CH}_3\text{NH}_3\text{PbI}_3$ films. Reproduced with permission.^{17,35}

GIXRD pictures of the decomposition of $\text{SiO}_2/\text{ZnO}/\text{CH}_3\text{NH}_3\text{PbI}_3$ films after heating at 100°C for various time periods in air. Fig. 4f shows the azimuthally integrated intensity plot as a function of the scattering vector (q) and time. From these ring patterns, it clearly revealed that the perovskite was degraded after heating at 100°C for *ca.* 13 min, and PbI_2 was immediately formed without any intermediates.

Hu *et al.* reported an *in situ* electrical resistance measurement combined with a time-resolved X-ray diffraction (XRD) analysis to study the interaction between perovskite materials with moisture exposed for a short- and a long-time.⁶⁶ They found that the perovskite films can be recovered from the short-time exposure, while the long-time exposure caused an irreversible decomposition of $\text{CH}_3\text{NH}_3\text{PbI}_{3-x}\text{Cl}_x$ into PbI_2 . They further identified that the perovskite films with less defects would be more stable to resist moisture. Divitini *et al.* investigated the heat-induced degradation of PSCs *via* transmission electron microscopy (TEM) with an *in situ* heating facility.⁶⁷ They confirmed that the thermal stability of the PSCs was influenced by the morphological changes of the perovskite films and the heat induced ion (iodine and lead) migration.

The surface properties of perovskites and PSCs during degradation processes can be investigated *via* photoelectron spectroscopy (PES). PES studies the surface chemical composition and the electronic structure by analyzing the kinetic energy of the emitted photoelectrons from the surface of the sample. Philippe *et al.* reported the electronic structure properties of the perovskite materials of $\text{CH}_3\text{NH}_3\text{PbI}_3$, $\text{CH}_3\text{NH}_3\text{PbI}_{3-x}\text{Cl}_x$ and $\text{CH}_3\text{NH}_3\text{PbCl}_3$ *via* a PES study.⁶⁸ The surface composition changes of the perovskite $\text{CH}_3\text{NH}_3\text{PbI}_3$ under effects of water, temperature, and storage time in air and argon were monitored by PES. It revealed that the decomposition of $\text{CH}_3\text{NH}_3\text{PbI}_3$ not only correlated with high humidity, but also with the temperature. It proved that a slow degradation of $\text{CH}_3\text{NH}_3\text{PbI}_3$ happened even in an inert atmosphere, like argon.

Electrochemical impedance spectroscopy (EIS) is an effective technique broadly applied to study various kinds of solar cells, for example DSSCs, OPSCs and PSCs. Information including the chemical capacitance, C_{it} ; the recombination resistance, R_{rec} ; the transport resistance, R_{tr} ; the charge transfer resistance, R_{CT} ; the electron lifetime, τ_n *etc.* can be extracted from Nyquist plots by fitting suitable equivalent circuit models.⁶⁹ The stability of perovskite materials and PSCs can be studied by EIS as well. Venkataraman *et al.* researched the photo-induced ion transport and degradation in perovskite active layers *via* measurements of EIS and powder XRD.⁷⁰ Three types of lead triiodide perovskites with M cations of methylammonium (MA^+), formamidinium (FA^+), and $\text{MA}_x\text{FA}_{1-x}$, respectively, were used as the active layers in PSCs for the EIS study at different temperatures under light illumination. They found that the degradation of the PSCs happened when light was illuminated in the region of IR and visible. They also showed a quasi-reversible photo-induced degradation existed in these active layers. An approach for the stability improvement of PSCs was proposed to incorporate a large FA cation with a small MA cation to avoid the phase changes and enlarge the active energy barrier for the ion transport.

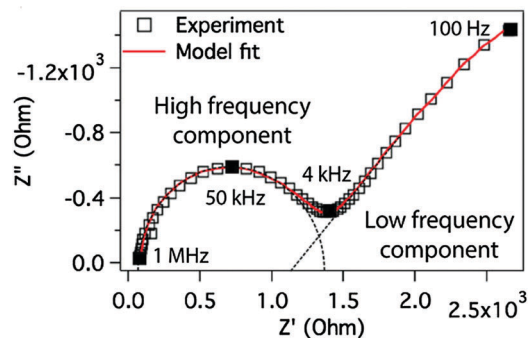


Fig. 5 EIS study of the $\text{CH}_3\text{NH}_3\text{PbI}_3$ sample at 45°C at 100 mW cm^{-2} light intensity. Reproduced with permission.⁷⁰

Fig. 5 shows the EIS plot of the $\text{CH}_3\text{NH}_3\text{PbI}_3$ sample tested under 100 mA cm^{-2} light illumination at 45°C and an applied bias of 0 V . Two distinct semicircles represented two charge transport regimes that can be clearly distinguished. Semicircles close to the region of origin can be assigned to the impedance arising from the electronic transport in the high frequency spectrum. The second semicircle presented increasing impedance due to charge or mass transfer at the interface or Warburg ion diffusion.

Thermal and mechanical measurements are worthy of attention for the degradation study of PSCs. PSCs may endure thermal and mechanical degradations in outdoor applications. Thermal gravimetric analysis (TGA) is used to study the thermal stability of perovskites by mass loss.⁷¹ The mechanical properties of stiffness and brittleness of perovskite films and PSCs affect the long-term stability of PSCs, especially in the case of flexible PSCs. The mechanical properties can be studied by the tension and fatigue tests.

An accelerated current-voltage (I - V) measurement as a function of duration time can test the long-term stability of PSCs, combining the thermal, humidity cycles, aging test facilities or concentrated sunlight. Stability test conditions for PSCs were recommended by Grätzel,⁷² and the suggested stability evaluation of PSCs included light soaking tests for 1000 h in full sunlight, and damp heat tests for 1000 h at 85% humidity and 85°C . The PSC test usually undergoes a hysteresis effect, and inconsistent results were obtained with the applied bias direction (*i.e.* forward scan, reversed scan) and scan rate. Kamat *et al.* recommended a protocol to characterize the PSC performance for accurate comparison.⁷³ Accurate and reliable performance characterization of PSCs is strongly needed for consistent comparison in the PSC research community.

3.2 Theoretical calculations

A number of theoretical studies illustrated how perovskite films degraded, and how perovskites interacted with environmental factors, directing fundamental understanding of the degradation processes of perovskite films.⁷⁴ The degradation of perovskite materials or interactions of perovskites with environmental species can be theoretically calculated at the molecular or single crystal level.^{75,76} The electronic structure of perovskites can be acquired by first-principles, *ab initio* and density functional

theory (DFT) methods. The properties of the bandgap, transition dipole moment, effective mass of carriers, defect levels, crystal structure, interaction energy, charge distribution and other parameters can also be obtained from a theoretical viewpoint. A combined study of experiment and theoretical calculations effectively elucidated the degradation problems of perovskites.⁷⁷

Angelis *et al.* published an atomistic study of MAPbI₃ interacting with liquid water using *ab initio* molecular dynamics simulations.⁷⁸ It was found that a fast solvation process occurred on the MAI-terminated surface because of the interaction of the water molecules with Pb atoms. The PbI₂-terminated surface was comparatively more stable than the MAI-terminated one, due to a strong bond of Pb–I on the facets. Surface hydration might happen on both MAI- and PbI₂-terminated slabs, and it showed no effect on the electronic structure of MAI-terminated slabs. However, surface hydration did enlarge the local band gap of the PbI₂-terminated slabs in the interfacial region. It showed that water incorporation into MAPbI₃ did not change the tetragonal structure of perovskite crystals with only around 1% volume expansion, and it slightly opened the band gap of MAPbI₃ crystals. They concluded that the new interfacial modification and device configuration could lead to a stable device for future commercial applications. Their work well illustrates the electronic and crystal structure properties at the interface of perovskite/water at the atomistic level.

Sit *et al.* studied the interaction of water, hydroxyl radicals and hydroxide ions with the tetragonal CH₃NH₃PbI₃ and CH₃NH₃PbBr₃ (110) surfaces by the *ab initio* DFT calculations.⁷⁹ The computational results revealed that CH₃NH₃⁺ (MA) cations favorably oriented with the NH₃ group, thus forming hydrogen bonds between the hydrogen ions of the NH₃ group and the halide ions. They also found that the degradation of the perovskites involved a vital step of desorption of CH₃NH₂ molecules, which may be considered as the beginning of perovskite degradation. The desorption energy was only slightly decreased by the water molecules, while it was significantly lowered by the interaction of the perovskite with the OH radical and the OH[−] ions. The PbI_x termination dependence on the tetragonal CH₃NH₃PbI₃ surfaces of (110), (001), (100) and (101) was studied *via* DFT calculations by Tateyama *et al.*⁸⁰ They revealed that the vacant termination was more stable than the PbI₂-rich flat one. Walsh *et al.* reported the origins of the high performance of PSCs by electronic structure calculations and discussed the possible degradation mechanisms of perovskites in the presence of water.⁸¹

Mobile ion diffusion has been considered as an important mechanism related to the aging and the hysteresis effects of PSCs.⁸² Tateyama *et al.* calculated the activation energies of the ion vacancy migrations in two kinds of perovskite materials of tetragonal CH₃NH₃PbI₃ (MAPbI₃) and trigonal (NH₂)₂CHPbI₃ (FAPbI₃) by a first-principles study.⁸³ The diffusion effects of anions and cations were studied. They discovered that I[−] anions can diffuse facilely with an energy barrier of *ca.* 0.45 eV for two perovskite materials, meanwhile, cation molecules of MA⁺ and FA⁺ can also migrate with an energy barrier of *ca.* 0.60 eV, indicating that cations can move under an applied bias as well.

They further identified that cation migration had negative effects on the lattice distortion and shrinkage, leading to damage of the perovskite crystal structure. They concluded that a larger cation and a lower defect concentration in crystal grains would be beneficial to suppress hysteresis and overcome the device aging problem.

Theoretical calculations study the degradation phenomenon of perovskite materials from the aspects of electronic and crystal structure. Particularly various interfaces of perovskite/metal oxides and perovskite/environmental factors have merits to study for improved organometallic perovskites and superior device architectures.

4. Approaches to improve the long-term stability of perovskite solar cells

The photovoltaic performance and long-term stability of PSCs mainly rely on the properties of perovskites, ETLs, HTLs, electrodes, device architecture, fabrication procedures, and so on. To overcome the instability problem of perovskite materials and produce stable PSCs, various approaches have been investigated, including perovskite material engineering, for example changing perovskite composition or alloying perovskites, designing 2D layered perovskites, or using all inorganic perovskites, *etc.* Other solutions for making stable PSCs involve using alternative organic or inorganic HTMs, and applying substituted electrode materials. Especially carbon based counter electrodes have become a very active research branch in the PSC field, bringing PSCs in a HTM-free, stable and cost-effective direction. Moreover, novel device configurations and robust encapsulation technologies all provide useful methods for constructing much more stable and reliable PSCs for practical applications. Based on the previous discussion and understanding of the degradation mechanism of perovskites and PSCs, various aspects are presented as follows for enhancing the long-term stability of perovskite materials and PSCs.

4.1 Engineering of perovskite materials

(a) **Perovskites with mixed cations or mixed halides (sometimes also called perovskite alloys).** The perovskite material has a general formula of AMX₃, whose three components “A”, “M” and “X” can be adjusted from chemical composition engineering to form numerous categories of perovskite materials. Thus, stable perovskites can be obtained through rational substitution of appropriate cations or anions.²³ For the organic cation “A” position, commonly used methylammonium (MA) can be replaced by or partially alloyed with other organic or inorganic cations. Halide “X” site can be filled by a single halide anion or mixed halide anions. The stabilities of the perovskites with these mixed cations or mixed halides mainly depend on their chemical composition associated crystal structure phase changes and their crystal distortions.

Han *et al.* prepared a perovskite material (5-AVA)_x(MA)_{1−x}PbI₃ by partially replacing the MA with 5-aninvaleric (5-AVA) in the cuboctahedral site of typical MAPbI₃.⁸⁴ Solar cells based on the

substituted compound demonstrated excellent long-term stability for more than 1000 h in ambient air under full sunlight illumination. The improved stability of the PSCs was attributed to a better surface contact of the perovskite $(5\text{-AVA})_x(\text{MA})_{1-x}\text{PbI}_3$ with TiO_2 and its lower concentration of defects than that of MAPbI_3 . Yang *et al.* reported a surface modified perovskite *via* hydrophobic tertiary and quaternary alkyl ammonium cations to gain moisture invasion.⁸⁵ It functions as a blocking layer to protect perovskites under a high relative humidity of $90 \pm 5\%$ over 30 days.

Formamidinium methylammonium lead iodide (FAPbI_3) has drawn extensive research interest due to its excellent optical and chemical stability. FAPbI_3 has a bandgap of 1.48 eV and an absorption edge of 840 nm,^{86,87} FAPbI_3 also has a higher onset decomposition temperature than MAPbI_3 as reported by Zhu *et al.*,⁸⁸ which may attribute to improved hydrogen bonding between the FA cations and the iodide ions of the Pb-I octahedra. Formamidinium (FA) cations have been used to mix with other organic or inorganic cations to tune the properties of perovskites. PSCs fabricated by $(\text{FAPbI}_3)_x(\text{MAPbBr}_3)_{1-x}$ achieved a high PCE of 20%.⁴² It was found that doping of MAPbBr_3 in FAPbI_3 or partially substituting FA with MA cations in FAPbI_3 can stabilize the α -phase of FAPbI_3 .^{89,90} Yi *et al.* developed a mixed A-site of perovskite ABX_3 by adding Cs cations to FAPbI_3 , and the as-fabricated PSCs with a mixed composition of a $\text{Cs}_{0.2}\text{FA}_{0.8}\text{PbI}_{2.84}\text{Br}_{0.16}$ absorber obtained a high PCE of over 17% and enhanced long-term stability in ambient air.⁹¹

Zhu *et al.* studied stabilizing the perovskite structure by tuning the tolerance factor t from alloying FAPbI_3 (a larger t) with CsPbI_3 (a small t).⁹² The $\text{FA}_{1-x}\text{Cs}_x\text{PbI}_3$ alloy and its corresponding solar cells showed improved humidity stability

compared to that of FAPbI_3 due to a more stabilized perovskite crystal structure. Fig. 6(a) shows the calculated formation energy difference as a function of the tolerance factor (t) and the Cs ratios of the $\text{FA}_{1-x}\text{Cs}_x\text{PbI}_3$ alloy. FAPbI_3 with the hexagonal structure had the lowest formation energy which indicated that it had a more thermodynamically stable crystal phase. As the Cs ratio increased from 0% to about 30%, a stable structure changed from the hexagonal (δ_{H}) to the orthorhombic (δ_0) phase with a minimum energy required for the phase changes from the cubic (α) phase to the two δ phase. Fig. 6(b) shows photo images of thin films of FAPbI_3 (left) and $\text{FA}_{0.85}\text{Cs}_{0.15}\text{PbI}_3$ (right) under 90% humidity conditions. $\text{FA}_{0.85}\text{Cs}_{0.15}\text{PbI}_3$ showed better humidity and thermal stabilities than FAPbI_3 , as $\text{FA}_{0.85}\text{Cs}_{0.15}\text{PbI}_3$ films did not undergo obvious color changes during aging. FAPbI_3 had a reversible phase change at the temperature of 170°C as the film color recovered. The photo-stability of single crystal nanowire shaped FAPbI_3 , MABr-stabilized FAPbI_3 , FAPbBr_3 , $(\text{FA},\text{MA})\text{PbI}_3$ alloys, and $(\text{FA},\text{MA})\text{Pb}(\text{Br},\text{I})_3$ was also reported.⁸⁸ FA based perovskites showed better photo-stability than MA substituted perovskites.

Mixed halide perovskites have been extensively studied to adjust the bandgap of perovskites for broad light absorption or for making colorful PSCs.^{23,93} The stabilities of mixed halide perovskites depend on the chemical composition and categories of halide atoms.²³ The humidity stability of perovskite crystals is mostly associated with dense packing and crystal structure. Due to the different ion radius and the electronic mass of Cl, Br, and I, a perovskite crystal structure substituted by a smaller halide atom would change from the tetragonal (pseudocubic) phase to the cubic phase. Smaller lattice constants and better humidity

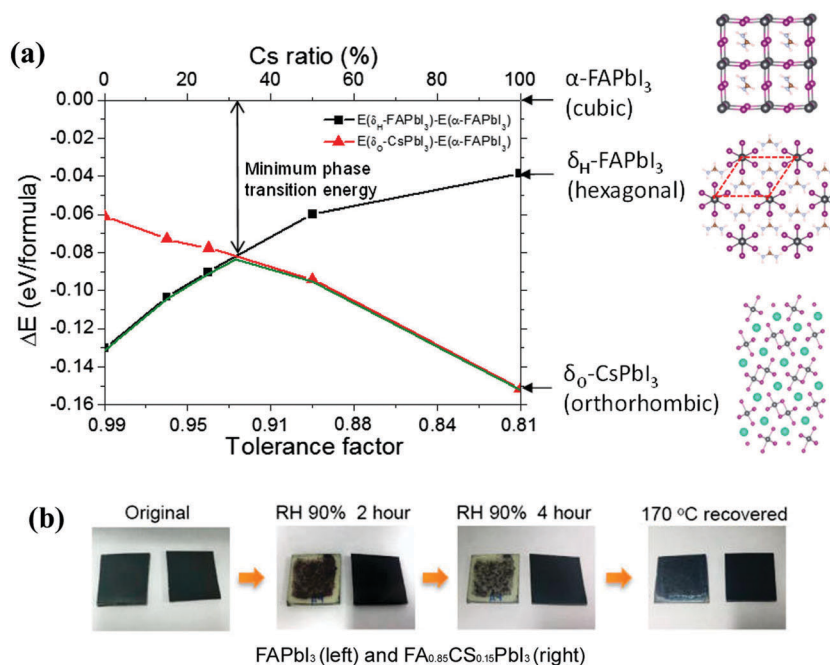


Fig. 6 (a) Calculated formation energy difference as a function of tolerance factor (t) and Cs ratios correlated with different phases of α -phase and δ -phases for $\text{FA}_{1-x}\text{Cs}_x\text{PbI}_3$ alloys, and (b) photos of thin films of FAPbI_3 (left) and $\text{FA}_{0.85}\text{Cs}_{0.15}\text{PbI}_3$ (right) under 90% humidity conditions. Reproduced with permission.⁹²

stability can be achieved after the above phase transition. Thus MAPbI₃ is known to be more sensitive to moisture compared with MAPbBr.^{23,24}

(b) Layered perovskites. Layered perovskites also known as two-dimensional (2D) perovskites can be derived from 3D analogues by shearing certain structure planes.⁹⁴ It was noticed that 2D perovskites can easily form good films with better resistance to humidity than the 3D analogues.⁹⁵ Drawbacks of 2D perovskites include a large bandgap, spatial confinement of the structure, and strongly bound excitons with low mobility. Even facing these obstacles, Karunadasa *et al.* pioneered an investigation of a 2D perovskite (PEA)₂(MA)₂[Pb₃I₁₀] (PEA = C₆H₅(CH₂)₂NH₃⁺, MA = CH₃NH₃⁺) synthesized from a mixture of (PEA)I, (MA)I and PbI₂ in a stoichiometric ratio.⁹⁵ They fabricated planar solar cells using the 2D perovskite as the light absorber, and 4.73% PCE was achieved with a high V_{oc} up to 1.18 V. Humidity stability tests confirmed this 2D perovskite had remarkable moisture resistance without any significant changes after exposure at a relative humidity of 52% for 46 days. This result is encouraging for developing layered perovskites.

To date, only a few studies have reported the preparation of layered perovskites and their photovoltaic applications. Yang *et al.* prepared an atomically thin 2D perovskite sheet (C₄H₉NH₃)₂PbBr₄ *via* a solution phase growth method.⁹⁶ Single- and few-unit-cell-thick single-crystalline perovskite crystals were prepared. They found that these 2D crystals displayed an unusual structural relaxation and efficient photoluminescence. Yao *et al.* studied a 2D perovskite based on methyl- and polymeric-ammonium cations through compositional engineering.⁹⁷ A small amount of polymeric ammonium PEI-HI was added to PbI₂ for solar cell fabrication, and the as-obtained 2D perovskite material (MAPbI₃)_{1-x}[(PEI)₂PbI₄]_x and its corresponding solar cells showed improved moisture resistance. The same group also reported that an *in situ* generated layered perovskite (PEI)₂[PbI₄] was formed underneath the 3D MAPbX₃ films.⁹⁸

Layered perovskites have been demonstrated as a feasible method to reinforce the humidity stability of perovskite films. More research studies need to be carried out to further advance layered perovskite structure design, film preparation and correlated solar cell fabrication, thus enhancing the long-term

stability of perovskite materials and solar cells, especially the humidity resistance properties.

(c) All-inorganic perovskites. All-inorganic perovskites represent a group of materials without any organic cations on the 'A' site in the formula AMX₃. Inorganic perovskites are known to be more thermally stable than their organic-inorganic hybrid counterparts. Cesium lead trihalides (CsPbX₃)⁹⁹⁻¹⁰¹ and cesium tin trihalides (CsSnX₃)^{31,102} are two representative inorganic perovskites, and they have been applied as light absorbers in photovoltaics. Snaith *et al.* developed a low temperature phase transition method to stabilize cesium lead iodide CsPbI₃ in the black perovskite phase at room temperature.⁹⁹ They fabricated planar structured solar cells based on CsPbI₃ and obtained a maximum 2.9% PCE performance. Their work paves a way that thermally stable inorganic perovskites can be applied in optoelectronics and solar cells.

All-inorganic perovskites of cesium lead bromide CsPbBr₃ have been investigated. They have a direct bandgap of 2.3 eV, appearing not so promising from the light absorption range point of view. However, Cahen *et al.* demonstrated that CsPbBr₃ can achieve a comparable PCE performance to the MAPbBr₃ based solar cells.¹⁰⁰ They regarded that the organic cation was not essential for high performance PSCs. Recently, the same group compared the thermal stability of perovskite materials of MAPbBr₃ and CsPbBr₃, and they also studied the long-term stability of the solar cells assembled from these two perovskites.¹⁰¹ The TGA results showed that the inorganic CsPbBr₃ was much more stable than the organic substituted MAPbBr₃ as shown in Fig. 7(a). 6% conversion efficiency was achieved by the CsPbBr₃ absorber under AM1.5 illumination. Fig. 7(b) presents that CsPbBr₃ based solar cells performed a better stability than that of MAPbBr₃ during two weeks of aging study. The reasons for the excellent stability of CsPbBr₃ based solar cells may be attributed to a higher volatility of MABr, thus MABr can be more easily released than CsBr. Another reason might be the more hydrophilic character of MAPbBr compared with CsPbI₃. All-inorganic perovskites have been demonstrated to be potential candidates for light harvesting, particularly aiming at stable PSCs.

Table 1 summarizes several representative organic-inorganic hybrid perovskites and all-inorganic perovskites used in the PSC

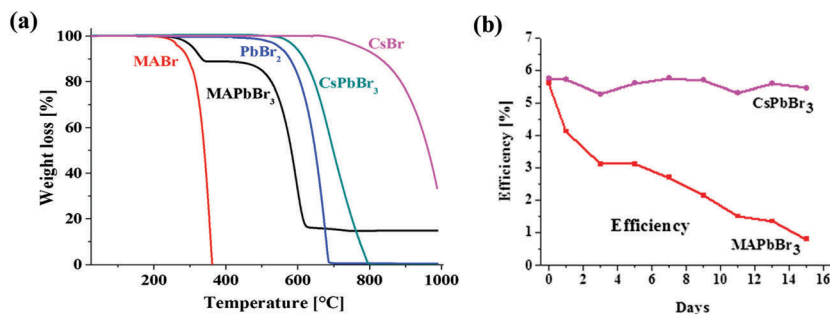


Fig. 7 (a) Thermogravimetric analyses of methylammonium bromide (CH₃NH₃Br), methylammonium lead bromide (CH₃NH₃PbBr₃), lead bromide (PbBr₂), cesium bromide (CsBr), and cesium lead bromide (CsPbBr₃); and (b) long-term stability study of CsPbBr₃-based and CH₃NH₃PbBr₃-based PSCs. Reproduced with permission.¹⁰¹

Table 1 Summary of several representative perovskite materials used in PSCs with their solar cell architecture, device performance and long-term stabilities

| Perovskite light absorbers | Device configuration | Max PCE (%) | Long-term stability; remaining PCE | Test conditions | Ref. |
|--|---|-------------|------------------------------------|--|-------------|
| CH ₃ NH ₃ PbI ₃ | FTO/c-TiO ₂ /meso-TiO ₂ /CH ₃ NH ₃ PbI ₃ /Spiro-OMeTAD/Au | 9.7 | 500 h; stable | R.T., air, without encapsulation, AM 1.5G | 39 |
| | FTO/c-TiO ₂ /meso-TiO ₂ /CH ₃ NH ₃ PbI ₃ /Spiro-OMeTAD/Au | 15 | 500 h; > 80% | 45 °C, 100 mW cm ⁻² light soaking, encapsulated | 40 |
| | FTO/c-TiO ₂ /meso-TiO ₂ /CH ₃ NH ₃ PbI ₃ (carbon)/carbon | 11.02 | 720 h; 83% | Stored in dry air with RH of 20% without encapsulation | 152 |
| | ITO/NiO _x /CH ₃ NH ₃ PbI ₃ /ZnO/Al | 16.1 | 1440 h; 90% | Tested: R.T., air, without encapsulation, RH of 30–50%; stored: air, R.T. | 9 |
| CH ₃ NH ₃ PbBr ₃ | FTO/c-TiO ₂ /CH ₃ NH ₃ PbBr ₃ /PIF8-TAA/Au | 10.40 | — | — | 168 |
| | FTO/c-TiO ₂ /meso-TiO ₂ /CH ₃ NH ₃ PbBr ₃ /PTAA/Au | 6.6 | 336 h; 15% | Tested: air, RH of 60–70%; stored: dark, air, RH of 15–20% | 102 |
| CH ₃ NH ₃ PbI _{3-x} Cl _x | FTO/c-TiO ₂ /Al ₂ O ₃ /CH ₃ NH ₃ PbI _{3-x} Cl _x /Spiro-OMeTAD/Au | ~ 11 | 1000 h; 55% | 40 °C at N ₂ , encapsulated, no UV cut-off filter, 76.5 mW cm ⁻² | 169 |
| (FAPbI ₃) _x (MAPbBr ₃) _{1-x} | FTO/c-TiO ₂ /meso-TiO ₂ /(FAPbI ₃) _x (MAPbBr ₃) _{1-x} /PTAA/Au | 20.11 | — | — | 42 |
| (5-AVA) _x (MA) _{1-x} PbI ₃ | FTO/c-TiO ₂ /meso-TiO ₂ /ZnO ₂ /Carbon/(5-AVA) _x (MA) _{1-x} PbI ₃ | 12.84 | > 1000 | R.T., air | 84 |
| (PEA) ₂ (MA) ₂ [Pb ₃ I ₁₀] | FTO/c-TiO ₂ /(PEA) ₂ (MA) ₂ [Pb ₃ I ₁₀]/Spiro-OMeTAD/Au | 4.73 | — | — | 170 |
| CH ₃ NH ₃ SnI ₃ | FTO/c-TiO ₂ /meso-TiO ₂ /CH ₃ NH ₃ SnI ₃ /Spiro-OMeTAD/Au | 6 | — | — | 32 |
| CH ₃ NH ₃ SnIBr ₂ | FTO/c-TiO ₂ /meso-TiO ₂ /CH ₃ NH ₃ SnIBr ₂ /Spiro-OMeTAD/Au | 5.73 | Few hours | — | 30 |
| CsPbBr ₃ | FTO/c-TiO ₂ /meso-TiO ₂ /CsPbBr ₃ /PTAA/Au | 6.2 | 336 h; stable | Tested: air, RH of 60–70%; stored: dark, air, RH of 15–20% | 100 and 101 |
| CsPbI ₃ | ITO/PEDOT:PSS/CsPbI ₃ /PCBM/Ca/Al | 2.9 | — | — | 99 |

c-TiO₂: compact TiO₂ layer; meso-TiO₂: mesoporous TiO₂ layer; RH: relative humidity; R.T: room temperature.

field; their corresponding solar cell architecture, device performance and long-term stability results are listed for comparison as well.

4.2 Applications of alternative organic or inorganic HTMs

Hole-transporting materials (HTMs), especially expensive Spiro-OMeTAD and its doped form, are easily degraded as discussed in Section 2.2(b), which is often considered as an important mechanism for the degradation of PSCs. Spiro-OMeTAD films prepared using the spin-coating method usually have miniscule pinholes. A dense and pinhole-free Spiro-OMeTAD film can promote better device performance and stability.⁵⁵ In order to enhance the stability of PSCs and reduce the cell fabrication cost, numerous research studies have focused on designing and synthesizing alternative organic or inorganic HTMs to substitute expensive Spiro-OMeTAD. Less dopant and stable HTMs are the major ways for achieving stable PSCs.

(a) **Organic hole-transporting materials (Or-HTMs).** Organic HTMs include poly-(triarylamine) (PTAA),⁴² poly(3-hexylthiophene) (P3HT)^{103,104} and polyaniline (PANI),^{105,106} *etc.* that have been employed in PSCs to substitute Spiro-OMeTAD. Swetha *et al.* summarized a review on small organic molecules and conjugated polymer based HTMs in PSC applications.¹⁰⁷ According to molecular structure differences, organic HTMs can be classified as assorted types of spiro-, triphenyl-, carbazole-, quinolizino-, triptycene-, thiophene-, diketopyrrolopyrrole- (DPP), and so on.

An appropriate HOMO level matching with the perovskite, a high hole mobility, and good thermal and chemical stabilities are the prerequisites for HTMs for stable and efficient PSCs. Recent progress of organic HTMs for producing durable PSCs is introduced herein.

HTMs with various molecular structures have been investigated. N. Jeon *et al.* synthesized a series of pyrene-core arylamine derivatives to replace the spirobifluorene core as HTMs for PSC applications.¹⁰⁸ A PCE of 12.4% was achieved, which was comparable to that of Spiro-OMeTAD based cells having a 12.7% PCE. HTMs with conjugated quinolizino acridine¹⁰⁹ and a two-dimensionally expanded π -system around an azulene core¹¹⁰ were synthesized and applied as HTMs for high performance PSCs.

Undoped HTMs draw a lot of research interest since dopants may deteriorate HTMs faster and accelerate the degradation of PSCs. Kazim *et al.* reported a 6,13-bis(triisopropylsilylethynyl) pentacene as a potentially stable and cost-effective HTM for PSCs.¹¹¹ Solar cells assembled in its pristine form exhibited a higher PCE of 11.8% over those of its doped form with the LiTFSI dopant and *t*-BP additives, and it was also higher than that of a doped Spiro-OMeTAD/LiTFSI/*t*-BP mixture. Another spiro type of HTM was developed by Ganesan *et al.*⁵² The as-fabricated solar cells based on this new HTM showed a PCE of 12.74% without any dopant, comparable to that of a PCE of 13.44% doped by the cobalt additive FK209. Meanwhile,

this new spiro HTM gained much higher photovoltaic performance than that of pristine Spiro-OMeTAD HTM based solar cells under the same fabrication conditions.

A highly hydrophobic oligothiophene derivative named DR3TBDTT was synthesized by Xiao *et al.* and used as a HTM in PSCs.¹¹² A flow agent of polydimethylsiloxane (PDMS) was added into a DR3TBDTT solution to achieve a uniform and thin layer of HTM. $\text{CH}_3\text{NH}_3\text{PbI}_{3-x}\text{Cl}_x$ planar solar cells assembled with the DR3TBDTT/PDMS HTM without ion additives achieved an 8.8% PCE, which was similar to the one fabricated by Spiro/LiTFSI HTMs. The same group also reported an ion-electrolyte-free HTM of triphenylamine derivative N,N' -di(3-methylphenyl)- N,N' -diphenyl-4,4'-diaminobiphenyl (TPD), combined with a buffer layer of 1,4,5,8,9,11-hexaazatriphenylene-hexacarbonitrile (HAT-CN) inserted between the HTM and metal electrode.¹¹³ A HAT-CN agent led to improved hole extraction and a lower charge injection barrier at the interface of the HTMs and Au electrodes. The long-term stability of these dopant free PSCs was investigated and stable PSCs without encapsulation maintained 90% PCE after around 1000 h storage at a humidity less than 20% at room temperature in the dark.

Choi *et al.* published a star-shaped HTM with a bis-dimethylfluorenylamino moiety for PSC applications.¹¹⁴ They showed that a fused triphenylamine core was essential for improving the hole mobility and HTM stability. A maximum of 14.21% conversion efficiency was gained by the fused triphenylamine HTM based PSCs. The triphenylamine HTM had a comparable stability to the Spiro-OMeTAD HTM for 250 h testing under one sun illumination in air at room temperature. Abate *et al.* synthesized a silolothiophene-linked triphenylamine (Si-OMeTPA) HTM¹¹⁵ for PSC applications, and the stability of the solar cells was evaluated by monitoring the steady-state maximum power output of the cells under working conditions. The PSCs using Si-OMeTPAs demonstrated enhanced stability compared with the state-of-the-art spiro-OMeTAD HTM, attributed to the superior thermal stability of the Si-OMeTPA molecule.

Table 2 lists a summary of several representative organic HTMs with their molecular structures, and their corresponding solar cell performance and stability results.

(b) Inorganic hole-transporting materials (In-HTMs). Compared with organic HTMs, p-type inorganic semiconductors are more thermally robust, and they can be used as hole transporting layers in PSCs as well. Materials such as copper thiocyanate (CuSCN),¹¹⁶ copper iodide (CuI),^{117,118} lead(II) sulfide (PbS),^{119,120} nickel(II) oxide (NiO),¹²¹ nickel oxides (NiO_x),^{122–124} copper doped NiO_x,¹²⁵ copper indium sulfide (CuInS₂)¹²⁶ and copper zinc tin sulphide (Cu₂ZnSnS₄, CZTS),¹²⁷ *etc.* have shown promising properties as HTMs in PSCs. Inorganic HTMs are chosen based on suitable energy levels of their valence band (E_v) or the Fermi levels (E_F) matching with the perovskites and the electrodes. Inorganic HTMs also need to have high conductivity for hole collection and accessible solution processing procedures compatible with the perovskite layer underneath. Taking NiO_x as an example, NiO_x has a valence band (VB) of -5.4 eV¹²³ and a work function of 5.05 eV,⁹ aligning well with the LUMO level of the organometallic halide perovskite $\text{CH}_3\text{NH}_3\text{PbI}_3$ (-5.4 eV) for

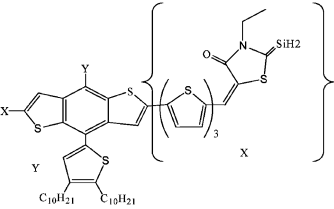
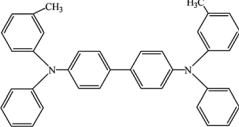
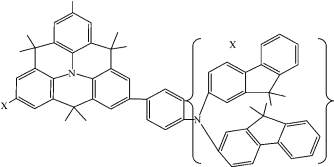
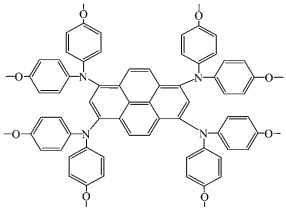
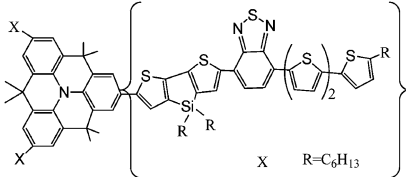
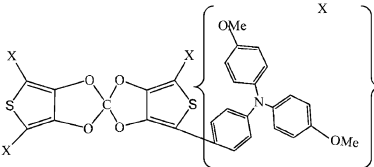
hole collection. Meanwhile, NiO_x has a conduction band (CB) as high as -1.8 eV,¹²³ efficiently blocking electron transport. Besides, NiO_x as a wide-bandgap metal oxide has excellent optical transparency. Thus it has been widely used as a HTM or an interfacial layer in PSCs. Here, recent progress on inorganic HTMs for enhanced stability studies of PSCs is presented.

A low temperature solution processed and cheap inorganic HTM of CuSCN was studied by Qin *et al.* for PSC applications.¹¹⁶ 12.4% PCE was obtained under full sunlight illumination, attributed to a predominantly higher hole mobility of CuSCN than that of Spiro-OMeTAD. It was also found that a thick perovskite $\text{CH}_3\text{NH}_3\text{PbI}_3$ film was necessary for high performance since the perovskite film can be partly dissolved by CuSCN. This work demonstrates that abundant and robust inorganic HTMs can confer high performance and cost-effective PSCs for reliable scale-up production.

Han *et al.* fabricated an inverted PSC with an aperture area larger than 1 cm² using heavily p-doped (p^+) NiMg(Li)O as a hole extraction layer and n-doped (n^+) Ti(Nb)O_x as an electron extraction layer as shown in Fig. 8.¹²⁸ Alloys of Li⁺ and Mg²⁺ co-doping NiO film supplied good lattice stability for Li_xMg_yNi_{1-x-y}O ternary oxides and provided increased electrical conductivity and reduced charge transport resistance, thus boosting hole extraction. In the inverted cell structure, the perovskite film was covered by stacked layers of PCBM and Ti(Nb)O_x, efficiently preventing moisture permeation. The resultant solar cell was encapsulated by covering glass with silver as the back contact, FTO as the front side, and sealed by UV-activated glue. The long-term stability of the PSCs was studied and 97% of the PCE remained after 1000 h storage in the dark. Less than 10% PCE was lost when the cell was exposed to sunlight for 1000 h under the short-circuit condition. This work demonstrated an excellent long-term stability and remarkable cell performance of 16.2% PCE for the large area PSC.

Several recent reports reported that NiO_x can be applied as an efficient inorganic HTM in PSCs. Yin *et al.* developed a pre-synthesized NiO_x nanoparticle solution for rigid and flexible PSC applications.^{129,130} Yang *et al.* reported a p-i-n structured PSC using p-type NiO_x as the HTM and n-type ZnO nanoparticles as the ETL.⁹ A maximum PCE of 16.1% was achieved. The solar cells showed an obviously enhanced stability against degradation of water and oxygen compared with cells fabricated with organic PEDOT:PSS as the HTM and PCBM as the acceptor. A remarkably stable performance was observed with 90% of the original PCE maintained after 60 days of storage in air at room temperature. It demonstrates that inorganic HTMs afford a promising and practical route for efficient and environmentally stable PSCs. Choy *et al.* explored a room-temperature processed pin-hole free NiO_x film as the HTM in PSCs.¹²³ 14.53% PCE was achieved for flexible PSCs, and 17.60% PCE for rigid ITO glass substrate based PSCs. The cell showed good stability over 30 days of storage with 93% of its initial performance maintained. Nejang *et al.* fabricated PSCs with the sputtered NiO_x as the HTM and Ni as the contact layer.¹²⁴ The cell presented a stable performance over 60 days. Surprisingly, this solar cell experienced a dramatically increasing PCE, starting

Table 2 Summary of several representative organic HTMs with their molecular structure, and their corresponding solar cell performance and stability results

| Chemical structure of HTMs | Name, max PCE, E_{LUMO} (eV), E_{HOMO} (eV) | PSC structure and long-term stability | Ref. |
|---|--|--|------|
|  | Oligothiophene derivative DR3TBDTT 8.8% −3.55, −5.39 | FTO/c-TiO ₂ /CH ₃ NH ₃ PbI _{3-x} Cl _x /DR3TBDTT + PDMS/Au (1) 313 h, 98% of PCE remained, stored under dark conditions in air at R.T. RH of 20%, 100 mW cm ⁻² simulated AM1.5G irradiation. Without encapsulation (2) 72 h, 91% of PCE remained. 100 mW cm ⁻² simulated AM1.5G irradiation, RH > 50% in air at R.T. Without encapsulation | 112 |
|  | Triphenylamine derivative TPD 7.1% −2.20, −5.38 | FTO/c-TiO ₂ /meso-TiO ₂ /CH ₃ NH ₃ PbI _{3-x} Cl _x /TPD/HAT-CN/Au 1000 h, 90% of PCE remained, without encapsulation, RH < 20% at R.T., in the dark | 113 |
|  | Fused triphenylamine based DMFA-FA 14.21% −2.23, −5.21 | FTO/c-TiO ₂ /meso-TiO ₂ /CH ₃ NH ₃ PbI ₃ /DMFA-FA/Au 250 h, 93% of PCE remained after aging at one sun illumination | 114 |
|  | Pyrene arylamine derivatives (Py-C) 12.4% −2.74 eV, −5.11 eV | FTO/c-TiO ₂ /meso-TiO ₂ /CH ₃ NH ₃ PbI ₃ /Py-C/Au stability: no report | 108 |
|  | Conjugated quinolino acridine based (Fused-F) 12.8% −3.66 eV, −5.23 eV | FTO/c-TiO ₂ /meso-TiO ₂ /CH ₃ NH ₃ PbI ₃ /Fused-F/Au thermal stability of Fused-F: stable and starts to degrade when the temperature is higher than 410 °C Device stability: no report | 109 |
|  | New spiro type PTS1 13.44% −2.40 eV, −5.15 eV | FTO/c-TiO ₂ /CH ₃ NH ₃ PbI ₃ /PTS1:FK209/Au 96 h, 95% of PCE remained, stored under ambient conditions without encapsulation | 52 |

from the initial PCE of 1.3% increasing to 7.28% after testing on the sixth day. The reason for this efficiency increase was attributed to the release of strain at the interface between the NiO_x and the perovskites. It may facilitate charge transportation and lead to a prominent increase of photocurrent density. Another reason might be that the resistivity of NiO_x decreased during storage, thus improving the carrier mobility.

Table 3 summarizes various inorganic hole-transporting materials (HTMs) used in PSCs, their photovoltaic performance and the long-term stability results are presented for comparison.

(c) Hole-transporting materials (HTMs) of carbon or carbon composites. Carbon nanomaterials have been extensively used in solar cells due to their superior properties. In PSCs, carbon and carbon composites can function as HTMs and

electrodes simultaneously. Snaith *et al.* studied P3HT functionalized single-walled carbon nanotubes (SWCNTs) incorporated with insulating polymers poly(methylmethacrylate) PMMA or polycarbonate (PC) matrices in PSCs.⁶³ Carbon nanotubes (CNTs) with a 1D nanostructure have excellent electrical conductivity and chemical stability. Compared with the organic HTM Spiro-OMeTAD and its doping mixture with LiTFSI, CNT/polymer based composite materials have higher water resistance at elevated temperatures. P3HT functionalization changed the electronic properties and solubility of SWCNTs, making them dissolve well in common solvents and form p-type forms for hole selection. Solar cells were fabricated by sequentially spin coating P3HT/SWCNT layers and an insulator of polymer layers. A maximum of 15.3% PCE was obtained with the HTL structure of P3HT/SWNT/PMMA. These PSCs demonstrated superior

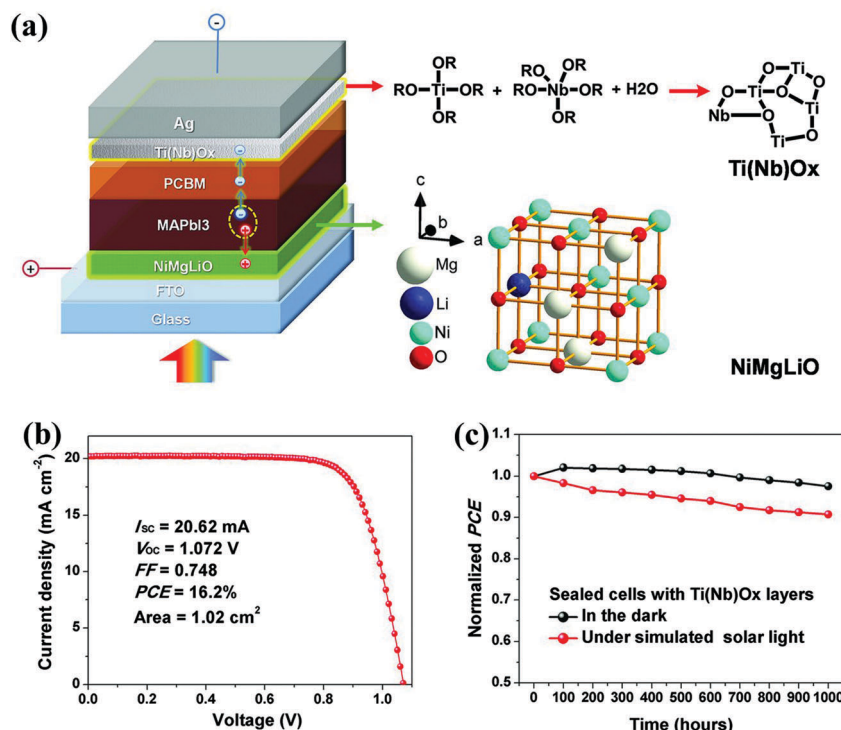


Fig. 8 (a) Configuration of solar cell FTO/NiMg(Li)O/CH₃NH₃PbI₃/Ti(Nb)O_x/PCBM/Ag with doped charge extraction layers of NiMg(Li)O and Ti(Nb)O_x and their crystal structure. (b) *J*-*V* curve of the best cell with an active area of 1.02 cm²; and (c) long-term stability study of encapsulated cells stored in the dark or under simulated light (AM 1.5, 100 mW cm⁻²). Reproduced with permission.¹²⁸

Table 3 Various inorganic hole-transporting materials (HTMs) used in perovskite solar cells with their photovoltaic performance and long-term stabilities

| Inorganic HTM | E_v or E_F (eV) | Device structure | Max PCE (%) | Stability, remaining PCE | Ref. |
|---|---------------------|---|-------------|---|------|
| CuSCN | -5.3 | FTO/c-TiO ₂ /meso-TiO ₂ /CH ₃ NH ₃ PbI ₃ /CuSCN/Au | 12.4 | — | 116 |
| CuI | -5.2 (E_v) | FTO/c-TiO ₂ /meso-TiO ₂ /CH ₃ NH ₃ PbI ₃ /CuI/Au | 6.0 | 1296 h; > ~75%; ambient conditions without encapsulation | 117 |
| CuInS ₂ | -5.05 | FTO/c-TiO ₂ /meso-TiO ₂ /CH ₃ NH ₃ PbI ₃ /CuInS ₂ /ZnS/Au | 8.38 | — | 126 |
| Cu ₂ ZnSnS ₄ (CZTS) | — | FTO/TiO ₂ /CH ₃ NH ₃ PbI ₃ /Cu ₂ ZnSnS ₄ /Au | 12.75 | 400 s, 0.7 V working conditions, stable | 127 |
| PbS | -5.1 | ITO/PbS CQDs/CH ₃ NH ₃ PbI ₃ /PCBM/Al | 7.5 | — | 119 |
| NiO | -5.1 (E_v) | FTO/c-TiO ₂ /ZrO ₂ /NiO/carbon(CH ₃ NH ₃ PbI ₃) | 14.9 | 1000 h, various test conditions | 121 |
| NiO _x | -5.4 (E_v) | ITO/NiO _x /CH ₃ NH ₃ PbI ₃ /C ₆₀ /Bis-C ₆₀ /Ag | 17.6 | 720 h, 93%, encapsulated stored in ambient air, dark conditions | 123 |
| NiO _x | -5.05 (E_F) | ITO/NiO _x /CH ₃ NH ₃ PbI ₃ /ZnO/Al | 16.1 | 1440 h, 90%, Tested: R.T., air, without encapsulation, RH = 30-50% | 9 |
| NiMg(Li)O | -5.25 | FTO/NiMg(Li)O/CH ₃ NH ₃ PbI ₃ /Ti(Nb)O _x /PCBM/Ag | 16.2 | 1000 h, 97%, (storage in the dark); 1000 h, 90% (under short-circuit conditions under full sunlight illumination) | 128 |

E_v : energy level of the valence band; E_F : work function; CQD: colloidal quantum dots.

stability under thermal stress. For both PMMA and PC cover layers, solar cells retained 80% of the initial PCE after being exposed to 80 °C in air for 96 h. Further raising temperature up to 100 °C caused an obvious cell performance degradation, which may be due to the structural damage of polymers heated at temperatures approaching their glass transition temperature (T_g). Attributed to good covering by the polymer, solar cells with PMMA and PC cover layers all exhibited excellent humidity stability in a water environment. The same group also explored polymer functionalized SWNTs combined with undoped Spiro-OMeTAD for better

charge extraction.¹²⁹ Two types of PSCs with a blend and a stack-layered of Spiro-OMeTAD and P3HT/SWNTs were fabricated separately for comparison. The layered structure showed comparable high efficiency to doped Spiro-OMeTAD with a maximum PCE of 15.4%. PSCs with the carbon and dropcasted Spiro-OMeTAD mixture as the HTM also showed excellent performance.¹³⁰

4.3 Interfacial modification

PSCs consist of two electrodes switched with an electron-transporting layer (ETL), a perovskite active layer and a

hole-transporting layer (HTL). As shown in Fig. 5, several interfaces exist in PSCs depending on the specific configuration of the cell. Research has revealed that interfaces between each layer in PSCs play a key role in carrier transport, charge extraction and charge recombination.^{19,131} Interfacial properties also lead to the degradation of perovskite materials and the performance decay of PSCs. Appropriate approaches to modify the interfaces between perovskite/ETL, perovskite/HTM, and electrode/adjacent layers are essentially crucial not only for high performance PSCs, but also for the long-term stabilities of PSCs.

(a) Interfaces of cathode/ETL/perovskite. TiO₂ films are broadly used ETLs in PSCs for both planar and mesoporous configurations. The interface properties of perovskite/TiO₂ ETLs affect interfacial charge recombination and charge transport. The interfacial characteristics of perovskite/TiO₂ films were investigated *via* a Kelvin force microscopy (KPFM) study by Qiao *et al.*¹³² They examined two kinds of back-recombination processes, one was at the interface of perovskite/TiO₂, and another was within the grain boundaries (GBs) of the perovskite itself. They found that PbI₂ films were formed during the film annealing due to the decomposition of CH₃NH₃PbI₃ films or uncompleted conversion of CH₃NH₃PbI₃ after reaction. They revealed that a suitable amount of PbI₂ films between CH₃NH₃PbI₃ and TiO₂ can build an energy barrier to decrease the back-recombination between the electrons from TiO₂ and the holes from perovskites. Their work draws a reasonable connection between perovskite fabrication procedures (*i.e.*, deposition and annealing process of perovskite films) and the interface properties of perovskite/TiO₂ ETLs.

An interfacial degradation study of an inverted planar lead halide PSC with various metal cathode contacts was reported by Guerrero *et al.*⁵⁹ Fig. 9 shows energy level diagrams of the PSCs at the interface of perovskite/cathode before and after degradation. Before contact, the energy levels of HTLs with their respective work functions Φ and the Fermi level of perovskite E_F are drawn in Fig. 9(a). Equilibrium is built along with energy level alignment after the function layers contact under dark conditions as shown in Fig. 9(b). A dipole layer is generated at the interface of perovskite/ETL/cathode, and it is readily separated by the internal and the external driving forces. In the case of degradation in the dark in Fig. 9(c), large dipoles exist at the interface of the perovskite and cathode, thus decreasing the applied potential for flat bands and causing a small V_{fb} ,¹³³ which is a value defined as the required voltage to generate a flat band in a semiconductor. Upon light illumination as shown in Fig. 9(d), the accumulation of photo-generated carriers cause more dipoles occupied at the interface of perovskite/cathode. This schematic illustration provides a basic understanding about the degradation of PSCs at the cathode/ETL/perovskite interface. It indicates that interfacial dipoles may be the main reasons for the device degradation and the low performance of PSCs. Judicious selection of ETLs, HTLs, metal contacts and interfacial layers can produce efficient and stable PSCs.

Interface engineering of ITO and TiO₂ in a planar structured PSC was studied by Yang *et al.*¹⁹ Both energy levels of ITO and

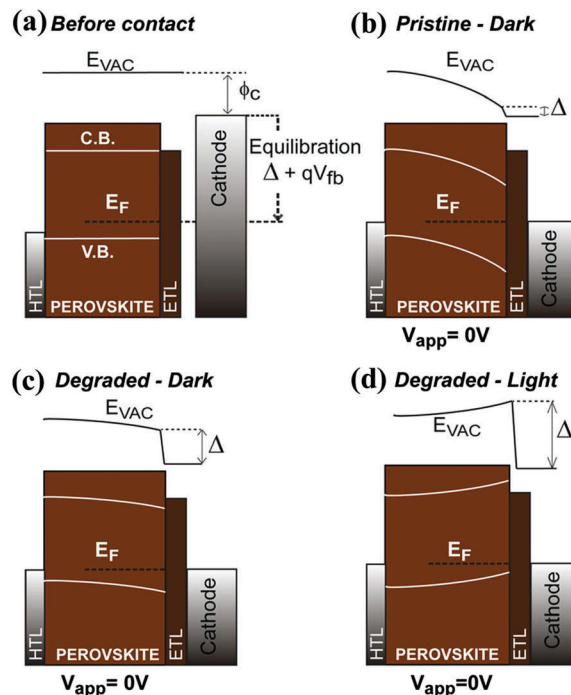


Fig. 9 Energy level diagrams of PSCs (a) before contact equilibrium; (b) after contact equilibrium under dark conditions; (c) degraded cells after contact equilibrium in the dark; (d) and illumination conditions. Reproduced with permission.⁵⁹

TiO₂ were well adjusted through surface modification, respectively, thus facilitating charge transport and improving charge extraction from ETLs to both sides of the contiguous layers. A poly-ethyleneimine ethoxylate (PEIE) with aliphatic amine groups was employed to lower the work function of ITO glass from -4.6 eV down to -4.0 eV, facilitating electron transport from the ETL to ITO. A TiO₂ ETL was modified by replacing the TiO₂ with yttrium-doped TiO₂ (Y-TiO₂), achieving an increased donor concentration and an improved conductivity of the ETL. The conduction band of Y-TiO₂ was well aligned with the LUMO energy level of the perovskites, leading to efficient charge extraction, minimized interfacial charge recombination, and reduced space charge depletion width at the interfaces of perovskite/ETLs.

Interfacial modifications between TiO₂ and perovskites were investigated to improve the photo-induced TiO₂ instability^{49,134} or reduce charge recombination.¹³⁵ Approaches adopted from quantum dot sensitized solar cells (QDSSCs) have been demonstrated to be effective methods for enhancing the photostability of PSCs. Ito *et al.* reported that Sb₂S₃ can be a surface blocking layer inserted between TiO₂ and CH₃NH₃PbI₃ by a chemical bath deposition (CBD) method.⁴⁹ PSCs with and without Sb₂S₃ interlayers were fabricated for comparison. They found that the performance of the un-encapsulated PSCs without the Sb₂S₃ decoration degraded to zero PCE in a very short time of 12 h, and the color of the CH₃NH₃PbI₃ films rapidly changed from black to yellow. However, the PSCs with an Sb₂S₃ interlayer showed more stable performance than those without the Sb₂S₃ layer under light illumination. Hwang *et al.* reported a core/shell structured TiO₂/CdS electrode prepared by a successive ionic layer

adsorption and reaction (SILAR) method to enhance the light stability of PSCs.¹³⁴ Intrinsic trap sites from the oxygen vacancies of the TiO_2 layer were restrained by the CdS layer. Light soaking experiments were conducted by continuously illuminating PSCs for 12 h. PSCs with the CdS surface passivation layer maintained around 80% of the initial PCE after full sun illumination of 12 h, while only 40% of the initial PCE was retained for the PSCs without the CdS layer. The improved photo-stability of the PSCs with the CdS layer was attributed to the suppression of trapping at the surface defects of TiO_2 , thus reducing the loss of charge recombination.

Interfaces between perovskite and ETLs may also affect the crystallization processes of perovskite layers, *i.e.*, the nucleation of perovskite grains and evaporation of residual volatile compounds. Thus the interface properties of ETL/perovskite may ultimately influence the quality of perovskite films and also affect the carrier injection and the charge transportation within bulk perovskites or at the interface of perovskite/ETLs. As well as TiO_2 ETLs, metal oxides including SnO_2 ,⁴⁴ WO_x ¹³⁶ and ternary oxide Zn_2SnO_4 (ZTO),¹³⁷ *etc.* were studied as ETLs in PSCs as well. Bera *et al.* fabricated a PSC using ZnSnO_4 as the ETL and perovskite $\text{CH}_3\text{NH}_3\text{PbI}_{3-x}\text{Cl}_x$ as the light absorber, and a high PCE up to 13.4% was obtained.¹³⁷ The as-assembled PSCs without any encapsulation presented a remarkably stable performance and 10% PCE remained after storage for more than a month in air.

(b) Interfaces of anode/HTL/perovskite. The interfaces of anode/HTL/perovskite have significant impact on the stability of perovskite materials and PSCs, since humidity and reactive species in air can penetrate from the anode and the HTM, then cause serious degradation of PSCs. A variety of methods have been reported to properly cover perovskite films either at the interface of perovskite/HTM or at the interface of HTM/anode. Yun *et al.* reported an interfacial layer of polyethyleneimine (PEI) incorporated between the perovskite films and the Spiro-OMeTAD HTM.¹³⁸ PEI with amine groups can bind with Pb metals and function as a compatibilizer at the interface of perovskites and HTMs. Delamination tests showed that a better adhesion at the interface of $\text{CH}_3\text{NH}_3\text{PbI}_3/\text{HTM}$ was realized after modification by PEI interlayers. The as-fabricated PSCs presented excellent moisture stability, and the cells without encapsulation maintained 85% of the initial efficiency for 14 days upon exposure to a relative humidity of 85%, attributed to an effective protection layer of PEI for preventing moisture intrusion.

The stability of PSCs largely relies on the interfacial properties of HTMs and electrodes. Snaith *et al.* revealed that an electrical shunting mechanism might be one possible reason for the fast performance decay of PSCs within the first few hundred hours of device operation.⁵⁸ Metal electrode ions may migrate into HTMs and finally contact with perovskite. To address this issue, they applied an insulating Al_2O_3 buffer layer infiltrated with the HTM between the perovskites and the metal contact. PSCs with Al_2O_3 buffer layers reduced the thickness of HTMs, decreasing the series resistance and enhancing the PCE of the resultant PSCs. The cells presented a stable performance

without degradation in the first 350 h under standard sunlight simulation. Kaltenbrunner *et al.* studied chromium oxide–chromium ($\text{Cr}_2\text{O}_3/\text{Cr}$) as an interlayer inserted between perovskite films and metal electrodes for air stable, light-weight flexible PSCs.¹³⁹ The interlayer of $\text{Cr}_2\text{O}_3/\text{Cr}$ improved the metal contact with better resistance to water and oxygen reactants, and it also avoided corrosive reaction between the iodine released by the perovskite with the metal electrodes. They fabricated flexible PSCs *via* a one-step transfer process of placing perovskite solar foils onto a stretchable acrylic elastomer. The as-assembled cells showed extraordinary mechanical flexibility and photovoltaic performance stability under compression and stretch tests. Fig. 10 shows solar cell images under compression and stretching tests, and I – V curves measured during the mechanical tests maintained relatively stable V_{oc} and FF, and only J_{sc} was decreased due to active cell area shrinking caused by mechanical deformation.

4.4 Application of substituted electrodes in PSCs: carbon or carbon composites

Expensive metal electrodes such as Au and Ag need to be deposited by thermal evaporation under high vacuum conditions, and thus are far from cost-effective for large-scale manufacturing. Metal electrodes with limited areas in PSCs cannot provide sufficient coverage on the top of perovskite materials as well. Alternative materials, especially carbon based electrodes, have become very promising research fields in PSCs,¹⁴⁰ resulting in strategies of HTM-free, stable, low-cost and printing-processable PSCs.

(a) Carbon based electrodes. Carbon is a low cost, easily processed, stable and abundant material. Carbon and its related composites have long been investigated as counter electrodes (CEs) in dye sensitized solar cells (DSSCs), achieving comparable conversion efficiency to platinum based CEs.^{141–143} With a work function of -5.0 eV similar to Au, carbon based CEs have been used to replace thermally evaporated Au and Ag in PSCs. A previous research study showed that PSCs fabricated by carbon CEs had better stability than metal based ones,^{144,145} due to the fact that carbon CEs are more inert to the perovskites and the environment, and they can offer larger areas to cover perovskite layers than metal electrodes.

A carbon material was firstly applied as the CE in PSCs by Han *et al.* in 2013.¹⁴⁶ A combination of carbon black and spheroidal graphite paste was prepared and used as the CE for mesoscopic methylammonium lead iodide ($\text{CH}_3\text{NH}_3\text{PbI}_3$) PSCs. 6.64% conversion efficiency was achieved and un-encapsulated PSCs showed stable performance without changes after storage in dry air under dark conditions for 840 h at room temperature. The same group also studied the size dependence of flaky graphite on PSC performance.¹⁴⁷ Graphite of different sizes was mixed with carbon black to prepare a screen-printing paste. It was found that the graphite size greatly affected the square resistance of the CEs. The filling properties of the perovskite precursors of PbI_2 and $\text{CH}_3\text{NH}_3\text{PbI}_3$ were influenced by the graphite size as well. It was discovered that carbon black combined with $8 \mu\text{m}$ graphite led to the highest PCE of more than 11%.

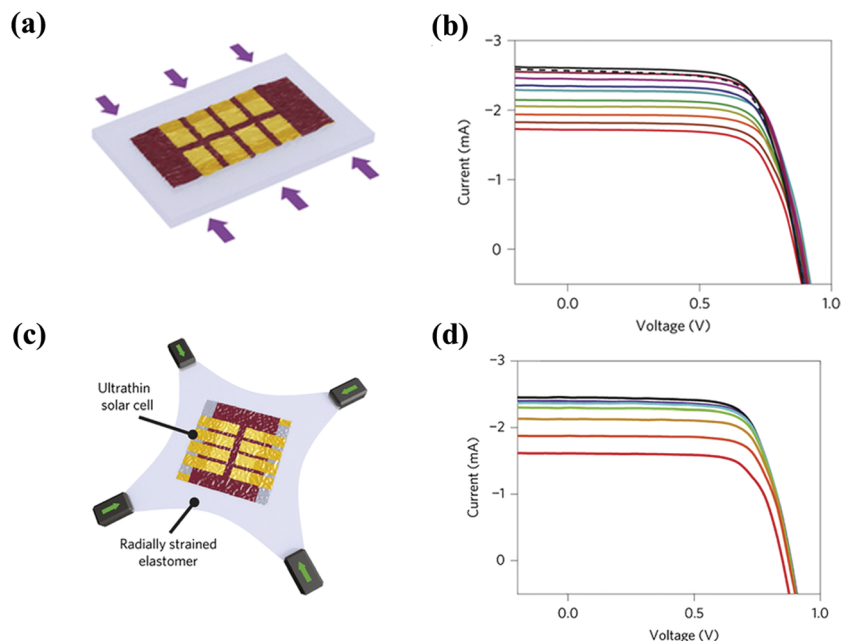


Fig. 10 (a) Schematic picture of a stretchable PSC under a compression stress test; (b) I - V characteristics of a PSC foil under compression in an interval of 10% down to 51% compressed; (c) schematic of radially stretchable PSCs under stretching, and (d) I - V characteristics of a PSC foil radially compressed to a 44% decrease in area. Reproduced with permission.¹³⁹

Another impressive result on carbon CE in PSCs was that a hole-conductor-free mesoscopic PSC with a light absorber $(5\text{-AVA})_x(\text{MA})_{1-x}\text{PbI}_3$ gained a 12.8% PCE.⁸⁴ The configuration of the PSC is shown in Fig. 11(a). Fig. 11(b) shows that $(5\text{-AVA})_x(\text{MA})_{1-x}\text{PbI}_3$ based PSCs obtained a higher current density-voltage characteristic than that of $\text{CH}_3\text{NH}_3\text{PbI}_3$. A PSC with $(5\text{-AVA})_x(\text{MA})_{1-x}\text{PbI}_3$ as the light absorber and carbon as the CE also presented a superior long-term stability for more than 1000 h in ambient air under full sunlight illumination. It was demonstrated that carbon materials can be very favorable CEs to improve the stability of PSCs.

Various carbon materials including carbon black,^{144,148} carbon nanotubes,¹⁴⁹ graphite,^{150,151} candle soot,¹⁵² graphene¹⁵³ or carbon/graphene composites¹⁵⁴ etc. have been successfully applied as CEs in PSCs. Yang *et al.* prepared an ink of carbon black mixed with $\text{CH}_3\text{NH}_3\text{I}$ for inkjet-printing PSCs.¹⁴⁸ $\text{CH}_3\text{NH}_3\text{PbI}_3$ was *in situ* formed within an interpenetrated carbon network, and a

continuous interface between perovskite and carbon ascribed to a high PCE of up to 11.60%. The long-term stability of the as-prepared PSCs without capsulation showed that the cell retained 90% of its maximum PCE after storage for 12 days at room temperature at a humidity of 30%. The same group reported a comparison study based on three representative carbon materials, *i.e.* carbon black, multi-walled carbon nanotubes (MWCNTs) and graphite.¹⁵⁰ They discovered that MWCNTs were the most superior HTMs among them due to a suitable size of 15 nm in diameter and a geometry of a 1D chain. 12.67% PCE with a remarkably high FF of 80% were gained by MWCNT based PSCs. Around 90% of their initial PCE was retained after storing one of the MWCNT PSCs in a 20% humidity chamber for 10 days. Ma *et al.* reported a low temperature processed conductive carbon paste for directly covering perovskite materials as the top electrode.^{144,145} Both TiO_2 mesoporous PSCs and ZnO based planar PSCs were

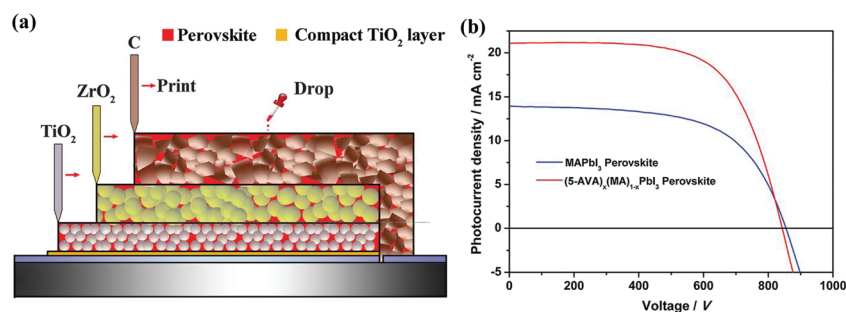


Fig. 11 (a) Schematic of a carbon CE based PSC, and (b) J - V characteristics of solar cells fabricated by MAPbI_3 and $(5\text{-AVA})_x(\text{MA})_{1-x}\text{PbI}_3$ as light absorbers under simulated AM 1.5 solar irradiation of 100 mW cm^{-2} at rt. Reproduced with permission.⁸⁴

fabricated with excellent cell performance and good long-term stability. The major reason was ascribed to the fact that a carbon CE with a hydrophobic surface can repel water penetration. They also found that the carbon based PSCs showed the best humidity stability compared with Au and Ag based PSCs. So far, we noticed that the highest PCE of carbon based PSCs in the literature studies achieved was 14.9% conversion efficiency as reported by Wang's group.¹²¹ The cell was fabricated using carbon as the electrode, $\text{CH}_3\text{NH}_3\text{PbI}_3$ as the light absorber, mesoporous TiO_2 and p-type NiO layers as the electron and the hole selective contacts respectively. The NiO HTM was given the credit for performance improvement which can efficiently extract charge to the external circuits. The stability of the solar cells was tested under different conditions to evaluate the effects of humidity, temperature and light exposure. They confirmed that light illumination had a greater influence on device stability than the condition of thermal aging at 60 °C. Li *et al.* reported a triple-layer mesoporous perovskite solar cell using carbon as a back contact.¹⁵⁵ Stability tests of indoor long time stability light soaking and outdoors in a hot desert climate were extensively studied. They found that the triplet layer cells remained stable under such aging conditions.

In HTM-free carbon based PSCs, device fabrication processes greatly impact the performance and stability of solar cells. Currently, there are three approaches to assemble carbon based PSCs as illustrated in Fig. 12. Fig. 12(a) shows a schematic of PSC fabricated by placing a carbon electrode on the top of a perovskite film. The stability of these types of devices may largely rely on the pristine properties of the carbon paste. Carbon pastes prepared by low temperature volatile solvents and nonreactive additives are preferred for stable PSCs. Fig. 12(b) presents a carbon based PSC with a carbon electrode formed in advance,

and then mixed perovskite precursors are filtrated *via* one step or two step routes, followed by film annealing to yield perovskite crystalline structures. A layer of insulator ZrO_2 is applied to prevent direct contact between TiO_2 and carbon. A carbon layer can be feasibly prepared and annealed without concern about damaging the perovskite films. Since perovskite precursors penetrate through the top side of the carbon film, the stability of these types of PSCs may relate to incomplete coverage of the perovskite films by the carbon films. Post treatment such as encapsulation may be beneficial for a stable device. The third approach is a so-called "chemical embedding method" developed by Yang's group. The PSCs are fabricated by properly clamping the anode and the cathode together as shown in Fig. 12(c). The active layer is generated by the reaction of PbI_2 /carbon films with methylammonium solution or methylammonium/carbon blends, followed by annealing to convert into a perovskite crystal structure. Evolution of this design originated from a simple clamping of two pieces of electrodes together from a variety of CE trials. The "chemical embedding method" produces perovskite films inside of the carbon porous films, thus good interface contact between the perovskite and the carbon electrode is expected to minimize interfacial charge accumulation and recombination loss. This fabrication produces sealed PSCs with two substrates intimately in contact with each other at the end, and the humidity stability of these types of PSCs may be enhanced.

So far, carbon based PSCs have achieved more than 14% PCE, still lower than metal based ones. The main advantage of carbon based PSCs is ascribed to their enhanced humidity stability. Even having excellent progress in the carbon CE based PSCs, the fundamental understanding about the degradation mechanism of carbon CE based PSCs, and questions about how to fully explore the hole extraction properties in the carbon based PSCs, and how to understand the hysteresis-free phenomenon in carbon based PSCs, continuously inspire researchers to move forward.¹⁵⁰

(b) Carbon/polymer composite electrodes. Hydrophobic polymers generally have large water contact angles and non-wetting nature. They can be blended with carbon materials to further boost the humidity resistance of PSCs. Epoxy, a typical hydrophobic polymer, functions as a binder to cement carbon nanoparticles. A counter electrode prepared by a carbon/epoxy composite with less void space can efficiently prevent humidity penetration. It can also promote better interfacial adhesion between the carbon and the perovskite. Therefore, incorporation of carbon with hydrophobic polymers has been shown to be an effective strategy to further advance the humidity stability of PSCs. Yang *et al.* studied hole-transporter-free PSCs fabricated by a $\text{CH}_3\text{NH}_3\text{PbI}_3$ light absorber, a mixture of carbon, epoxy and additives as the CE and the "water-rejecting barrier" simultaneously.¹⁵⁶ Solar cells based on the highly conductive carbon/epoxy paste CE achieved a PCE of 9.17%. A hydrophobic Ag paint was sequentially applied on the top of a carbon/epoxy film to restrict water intrusion and lower the series contact resistance. PSCs based on the carbon + epoxy/Ag CEs achieved a high PCE of 11% and displayed impressive waterproof

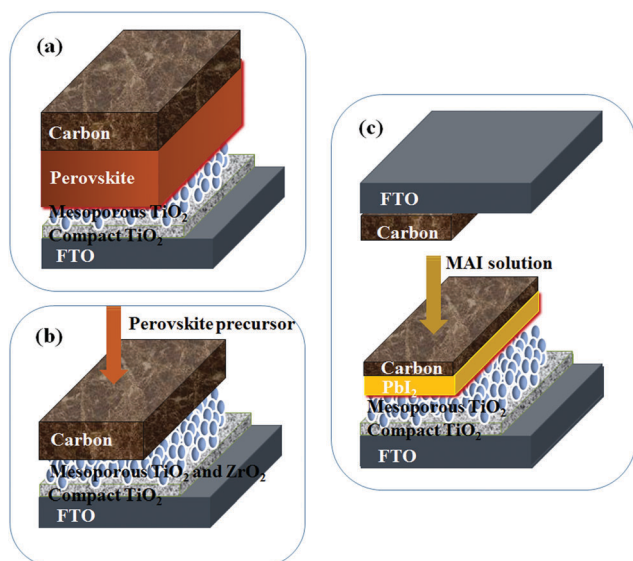


Fig. 12 Three different fabrication methods for carbon CE based PSCs: (a) the carbon electrode was covered on the top of perovskite films; (b) perovskite films were filtered into carbon films, and (c) "chemical embedding method" with carbon placed on PbI_2 films first and then interpenetrated with MAI solution, then the two electrodes were clamped together.

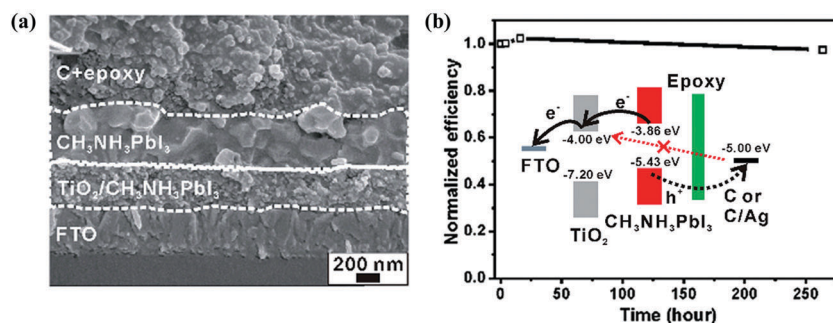


Fig. 13 (a) SEM cross-section image of PSCs using carbon and epoxy as the electrode, and (b) stability test of PSCs for a period of 250 h. The inserted figure shows the energy level diagram and electrons and holes flowing from the cell. Reproduced with permission.¹⁵⁶

properties with a stable performance for a period of 80 min even when immersed in water. The cell also maintained a stable photovoltaic performance at a high humidity of 70–90% and a thermal stress of 50 °C for 250 h without noticeable degradation. SEM cross section images of the as-prepared PSC are presented in Fig. 13(a), and the stability test of the cell is shown in Fig. 13(b) with an energy level diagram as an inset. Composites of carbon nanotubes/polymers as HTMs for PSC applications are discussed in Section 4.2(c).^{63,129} It demonstrated that carbon nanotubes had excellent hole extraction properties and can greatly enhance the humidity and thermal stability of PSCs. Table 4 comprehensively lists carbon materials used in PSCs with their device architecture, photovoltaic performance and long-term stabilities.

The stability of PSCs can be improved by applying a metal alloy as an alternative electrode.^{157,158} Commonly used metal electrodes in PSCs are Au, Ag, Al, *etc.*, however, metal ions can diffuse into HTMs or perovskite layers, thus causing film degradation or shunting. Jiang *et al.* reported an AgAl alloy electrode based inverted PSC with a cell structure of ITO/PEDOT:PSS/CH₃NH₃PbI₃/PCBM/electrode.¹⁵⁸ The cell made of an AgAl alloy electrode had a slightly higher PCE than that of an Ag electrode, and the V_{oc} of AgAl electrode based cells remained constant after 360 h of aging under a relative humidity of 10% in air. The reason for the improvement of stability may be due to the fact that the AlO_x interlayer preventing the Ag atoms from diffusing into the perovskite layer. The AlO_x layer may also result in an improved adhesion between the metal contact and PCBM, thus avoiding moisture invasion.

A counter electrode in PSCs is not only critical for charge collection, but also greatly influences the stability of PSCs. The CE works as a top window exposed to the outdoor environment. Hence, environmentally stable and water resistant CEs with superior electrical conductivity are expected to keep PSCs away from moisture and reactants attacking, and these CEs may apparently improve the long-term stability of PSCs.

4.5 Construction of PSCs by adding functional additives or scaffolds

In a typical PSC, the electrons and holes in the perovskites need to be efficiently transported by choosing appropriate charge transporting/selective layers. Apart from these charge transporting/selective

layers that closely interacted with the perovskite films, functional additives and scaffold layers, easily neglected parts in certain types of PSCs, can offer a vital balance for the perovskite films from exposure to the environment. New approaches using diverse materials and device structures different from the traditional dye sensitized solar cells (DSSCs) have been explored to fabricate novel structured and stable PSCs. These new designs add more choices to choose environmentally robust materials for reliable PSCs.

Grätzel *et al.* reported a surface treatment method using a bifunctional phosphonic acid ammonium additive to modify the surface of perovskite CH₃NH₃PbI₃.¹⁵⁹ The additive functions as a crosslinker to bridge the neighboring grains in the perovskite films, facilitating the perovskite crystal growth within the TiO₂ mesoporous films. This method significantly improved the PCE from 8.8% to 16.7%. Meanwhile, the moisture stability of the PSCs with butylphosphonic acid 4-ammonium additive (4-ABPA) was retained for 6 days at 55% humidity in the dark or under 10% simulated sunlight soaking, much more stable than the devices without a 4-ABPA crosslinker. Thermal stress tests at a temperature of 85 °C were carried out to evaluate the stability of the as-surface modified PSCs, and less than 20% of the PCE decreased after 350 h testing. This work proved that the 4-ABPA additive can effectively block moisture intrusion and slow down the degradation of the inner perovskite crystals.

Recently, Zhao *et al.* reported a new approach to fabricate PSCs by using an insulating hygroscopic polymer polyethylene glycol (PEG) as the scaffold.¹⁶⁰ The configuration of the solar cell is shown in Fig. 14(a). PSCs were fabricated by simply mixing PEG monomers (C₂H₄O), PbI₂ and CH₃NH₃I in a suitable molar ratio, and then the mixture of perovskite precursors and the scaffold was spin-coated onto 40 nm TiO₂ compact layers followed by annealing at 105 °C for 70 min. Spiro-OMeTAD and gold were used as the HTM and the top electrode, respectively, to complete the device fabrication. A stable PCE of up to 16% was achieved by this novel configuration. Amazingly, the cell presented an extraordinarily stable behavior at a humidity of 70% for 300 h. The cell presented irreversible “self-healing” properties recovered from water spray as shown in Fig. 14(b and c). This unique phenomenon might be attributed to the strong interaction of the PEG polymer with the perovskites. The hygroscopic PEG may act as a water absorber around the perovskite crystals, thus hindering water from

Table 4 Carbon based materials, device configurations and their photovoltaic performance and long-term stabilities in perovskite solar cells

| No. | Carbon materials | Device configuration | Max PCE (%) | Stability | Year | Ref. |
|-----|---|---|---------------|---|------|------|
| 1 | Carbon | FTO/c-TiO ₂ /meso-TiO ₂ /ZrO ₂ /NiO/C(CH ₃ NH ₃ PbI ₃) | 14.9 | 1000 h, 80% PCE remained, thermal aging at 60 °C in the dark | 2015 | 121 |
| 2 | Carbon | FTO/c-TiO ₂ /meso-TiO ₂ /Silane/ZrO ₂ /C(CH ₃ NH ₃ PbI ₃) | 12.7 | — | 2015 | 171 |
| 3 | Multi-walled carbon nanotubes (MWCNTs) | FTO/c-TiO ₂ /meso-TiO ₂ /CH ₃ NH ₃ PbI ₃ /C | 12.67 | 240 h, 90% PCE remained, stored in a 20% humidity chamber | 2015 | 150 |
| 4 | Carbon black/graphite power/ZrO ₂ | FTO/c-TiO ₂ /meso-TiO ₂ /ZrO ₂ /CH ₃ NH ₃ PbI ₃ /C | 11.63 | — | 2015 | 147 |
| 5 | Carbon | FTO/c-TiO ₂ /meso-TiO ₂ /mesoscopic NiO/C(CH ₃ NH ₃ PbI ₃) | 11.4 | 700 h, ~55% of PCE remained | 2015 | 172 |
| 6 | Carbon/epoxy | FTO/c-TiO ₂ /meso-TiO ₂ /CH ₃ NH ₃ PbI ₃ /C+epoxy/Ag paint | 11 | 250 h, stable, stored in humidity of 70–90% and 50 °C thermal stress | 2015 | 156 |
| 7 | Conductive carbon | FTO/c-ZnO/CH ₃ NH ₃ PbI ₃ /C PEN/ITO/c-ZnO/CH ₃ NH ₃ PbI ₃ /C | 8 4 | — 1000 times bending, 80% of PCE remained, stored in air, R.T. 100 mW cm ⁻² | 2015 | 157 |
| 8 | P3HT:Carbon nanotubes | FTO/c-TiO ₂ /meso-Al ₂ O ₃ /perovskite/P3HT:SWNTs/Spiro-OMeTAD/Ag | 15.4 | — | 2014 | 129 |
| 9 | P3HT:Carbon nanotubes | FTO/c-TiO ₂ /meso-Al ₂ O ₃ /CH ₃ NH ₃ PbI _{3-x} Cl _x /P3HT:SWNTs/PMMA/Ag | 15.3 | 96 h, 80% of PCE remained after exposed to 80 °C in air | 2014 | 63 |
| 10 | Carbon black/graphite | FTO/c-TiO ₂ /meso-TiO ₂ /ZrO ₂ /C((5-AVA) _x (MA) _{1-x} PbI ₃) | 12.8 | >1000 h, R.T., air | 2014 | 84 |
| 11 | Inkjet printing carbon black | FTO/c-TiO ₂ /CH ₃ NH ₃ PbI ₃ /C | 11.60 | 288 h, 90% of PCE remained, stored in air at R.T., humidity ca. 30%, un-encapsulated | 2014 | 173 |
| 12 | Candle soot | FTO/c-TiO ₂ /meso-TiO ₂ /CH ₃ NH ₃ PbI ₃ /Candle soot | 11.02 | 720 h, ~85% of PCE remained; stored in dry air (20% moisture), un-encapsulated | 2014 | 152 |
| 13 | Carbon black/graphite | FTO/c-TiO ₂ /TiO ₂ (nanosheets)/ZrO ₂ /C(CH ₃ NH ₃ PbI ₃) FTO/c-TiO ₂ /TiO ₂ (nanoparticles)/ZrO ₂ /C(CH ₃ NH ₃ PbI ₃) | 10.64 7.36 | — — | 2014 | 174 |
| 14 | Mesoscopic carbon layer/flexible graphite sheet | FTO/c-TiO ₂ /meso-TiO ₂ /CH ₃ NH ₃ PbI ₃ /mesoscopic carbon layer/flexible graphite sheet | 10.2 | — | 2014 | 151 |
| 15 | Carbon nanotubes | FTO/c-TiO ₂ /meso-TiO ₂ /CH ₃ NH ₃ PbI ₃ /C FTO/c-TiO ₂ /meso-TiO ₂ /CH ₃ NH ₃ PbI ₃ /C+Spiro-OMeTAD | 6.87 9.90 | — — | 2014 | 149 |
| 16 | Conductive carbon | FTO/c-TiO ₂ /meso-TiO ₂ /CH ₃ NH ₃ PbI ₃ /C | 9 | >2000 h, in air under dark conditions, without encapsulation | 2014 | 144 |
| 17 | Carbon paste | FTO/c-TiO ₂ /meso-TiO ₂ /CH ₃ NH ₃ PbI ₃ /C | 8.31 | 800 h, stable, stored in air at R.T. without encapsulation, under one sun illumination | 2014 | 175 |
| 18 | Carbon black/spheroidal graphite | FTO/c-TiO ₂ /meso-TiO ₂ /ZrO ₂ /CH ₃ NH ₃ PbI ₃ /C | 6.64 | 840 h, 98% PCE is stable Stored in dry air at R.T. without encapsulation | 2013 | 146 |

permeating and reacting with the perovskites. Besides improved the humidity stability, light soaking experiments of the cells also distinguished that the PEG embedded PSCs had better resistance to light than that without the PEG scaffolds, due to the perovskite decomposition or I ion migration. When PEG was incorporated into the cells, a less humid environment may be realized, slowing down the photodecomposition of the perovskites. This work gives us an insight that the stability of PSCs can be enhanced not only by using hydrophobic polymers to cover perovskites, but also by applying hygroscopic polymers as a sponge to absorb water in the PSCs. Meanwhile, more mechanisms associated with this brand new scaffold need to be explored to fully explain charge transportation, interface interaction and enhanced stability properties.

4.6 Encapsulation or surface passivation of PSCs

Due to the sensitivity of perovskite materials to the outdoor environment, encapsulation or surface passivation of PSCs is an effective strategy to cut off the interaction of perovskites with environmental molecules. Lacking of operational stability is also a

big issue for organic polymer solar cells as comprehensively reviewed by Krebs *et al.*^{161,162} The approaches for efficient encapsulation of organic polymer solar cells may help to correlate the problems faced in the PSC field. Properly sealing PSCs using thermocuring epoxy glue can avoid moisture, oxygen or other environmental effects from degrading PSC performance. Shielding the PSC surface by covering glasses with UV cutoff filters can efficiently block UV radiation, thus oppressing the photo-induced degradation of PSCs. Recent progress of encapsulation or surface passivation to improve PSC degradation is introduced below.

A hydrophobic Teflon polymer layer spin-coated on the outside of PSCs for surface passivation was reported by Yong *et al.*¹⁶³ A PSC with a Teflon passivation layer showed a significant stability enhancement after 30 days of storage in ambient atmosphere, and around 95% of the original PCE was retained. Teflon coated perovskite films showed an unchanged XRD pattern in the XRD spectrum and a stable mass tested using quartz crystal microbalance measurements. Han *et al.* studied several encapsulation methods for decreasing the water

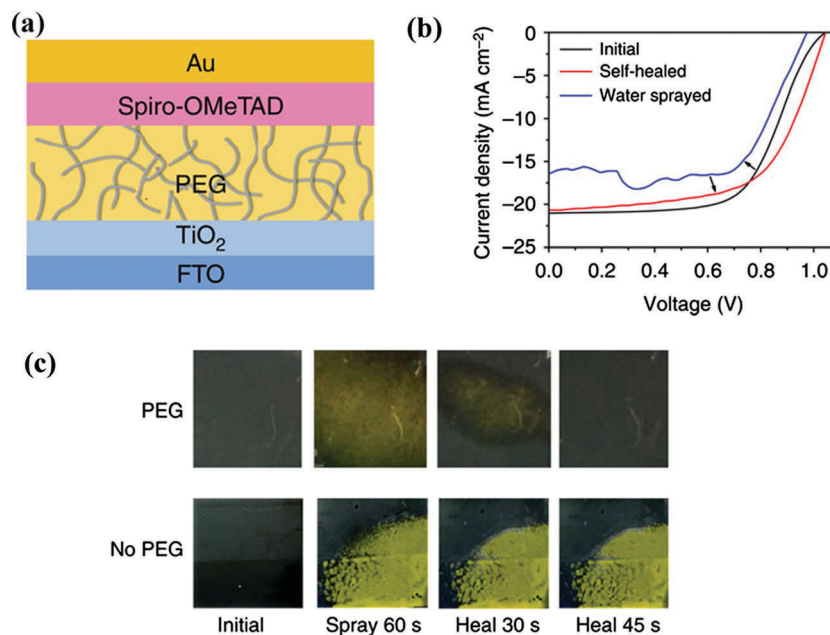


Fig. 14 (a) The architecture of a PSC using a polymer-scaffold; (b) J - V characteristics of PSCs at the initial, water sprayed and self-healed steps, and (c) photography of the perovskite films with and without a PEG scaffold after water-spraying for 60 s, and kept in air for 30 s and 45 s for self-healing. Reproduced with permission.¹⁶⁰

ingress in a planar PSC.¹⁶⁴ They researched the photovoltaic performance and the degradation processes of the encapsulated PSCs at a high temperature of up to 85 °C and humidity up to 80%. For the first time, Carlo *et al.* studied the long-term stability of solid state module based encapsulated PSCs.¹⁶⁵

Surface passivation methods have been explored to enhance the thermal and humidity stabilities of perovskite films and make PSCs more water resistant. A non-hydrolytic Al_2O_3 layer prepared by a water-free atomic layer deposition (ALD) method was applied on the top of the perovskite films.¹⁶⁶ The perovskite films with the protected Al_2O_3 films showed better thermal resistance up to 250 °C, and the moisture stability was ten times increased at a relative humidity (RH) of 85% than that without Al_2O_3 protection. Kang *et al.* reported a water-repellent PSC using a hierarchical pyramidal array of bifunctional polydimethylsiloxane (PDMS) films adhered to the FTO side of PSCs.¹⁶⁷ PDMS arrays were prepared from micro pyramid structures of a PET film mold, and followed by surface treatment of Ar ions and octafluorocyclobutane (C_4F_8) gas to form a thin elastic and superhydrophobic shell. The as-obtained PSCs presented good hydrophobicity and water repelling properties.

To further improve the device stability against moisture and harsh environments, appropriate encapsulation with water resistance, UV light protection and functional layers are definitely desired for circumventing the device performance decay and prolonging the life span of PSCs for practical applications.

5. Conclusions and outlook

Perovskite solar cells (PSCs) have experienced an unprecedented rapid development since perovskite materials were

firstly adopted into the photovoltaic field in 2009. Numerous research efforts have been made in the power conversion efficiency race and the highest conversion efficiency of PSCs has reached over 22.1% to date. Steady growth of this promising field suggests that it would be practically applied in households in the near future. Vast research expansion in PSCs covers perovskite crystal design and synthesis, perovskite film deposition, device fabrication, and fundamental understanding of device operation and degradation mechanisms. Knowledge acquired from dye sensitized solar cells (DSSCs), quantum dot solar cells (QDSCs), organic polymer solar cells (OPVs), inorganic semiconductors, compound solar cells, *etc.* has developed the PSC field at an extraordinarily fast pace. As a rising star of renewable energy resources, PSCs face a serious long-term stability problem, hindering their operation for a long period. Thus fully understanding the degradation mechanisms of perovskite materials and PSCs is urgent for developing stable PSCs. Challenges of PSC performance and long-term stability mainly rely on the effects of (1) the unstable nature of perovskite materials under conditions of humidity, thermal, UV light and O_2 ; (2) electron transporting layer (ETL) related degradation; (3) Spiro-OMeTAD HTM associated degradation; (4) metal electrode originated degradation, *etc.* In order to address these issues, we highlight the approaches to study the stability problems of perovskite materials and PSCs from the aspects of experimental observations and theoretical calculations. Furthermore, we focus on summarizing the available strategies to improve perovskite materials and device stability from perovskite material engineering, for example perovskite compositional changing or alloying; 2D layered perovskite preparation; and all-inorganic perovskite synthesis. To overcome device stability issues and produce a

stable PSC, various approaches are explored, including interfacial engineering to form a stable and efficient interface interaction, using alternative organic or inorganic HTMs, and substituting metal electrodes with environmental inert carbon materials and carbon composites. Moreover, novel device structure and robust encapsulation technologies provide meaningful solutions for constructing stable and reliable PSCs for real marketing.

Although the long-term stability of PSCs has drawn more and more research attention, still the fundamental understanding of rationally designed stable perovskite materials and making stable PSCs remains far from being comprehensively understood. The challenge of this critical issue can be identified from the following questions:

(1) How to minimize the structural defects of perovskite materials and prepare thermally and humidity stable perovskite crystals suitable for the broad wavelength region of light absorption? All-inorganic perovskite materials showed stable thermal stability, and rational designing of all-inorganic perovskite materials from the molecular engineering viewpoint may lead to a path for stable light harvesting materials in PSC applications.

(2) How to optimize interfacial layers specifically ETLs and HTLs to have a benign environment for perovskites, and meanwhile extract and transport charges with lower recombination loss? PSCs with stable HTLs or even without HTLs are good directions for stable cells. Appropriate interfacial treatment may also add benefits for lower charge recombination.

(3) How to develop stable inorganic lead-free perovskite materials, such as using inorganic double perovskites instead of traditional inorganic-organic hybrid perovskites? Lead-free perovskite is a promising research area for the benefit of our environment, and lead pollution may largely restrain the application of lead halide perovskites. Therefore, Sn replaced or new lead-free perovskites with double or even more complex structures are potential routes for stable and environmentally friendly PSCs.

With in-depth understanding of perovskite material degradation and device performance decay, proper material processing and device handling, technologies in PSCs will become more and more mature. High PCEs and stably performing PSCs are expected to be realized for terrestrial applications in the near future.

Acknowledgements

The authors sincerely thank financial support from the National Science Foundation of China (51502246), the Scientific Research Foundation for the Returned Overseas Chinese Scholars, the State Education Ministry, the Natural Science Basis Research Plan in Shaanxi Province of China (2015JQ5128), and the Fundamental Research Funds for the Central Universities (3102014JCQ01098). Grant support by a Grant-in-Aid for Scientific Research of (KAKENHI) program in Japan (C, Grant Number 15K05597) and a postdoctoral fellowship sponsored by the Kyushu Institute of Technology (KIT) of Japan are acknowledged as well.

Notes and references

- 1 N.-G. Park, *J. Phys. Chem. Lett.*, 2013, **4**, 2423–2429.
- 2 H.-S. Kim, S. H. Im and N.-G. Park, *J. Phys. Chem. C*, 2014, **118**, 5615–5625.
- 3 J. H. Rhee, C.-C. Chung and E. W.-G. Diau, *NPG Asia Mater.*, 2013, **5**, e68.
- 4 H. S. Jung and N.-G. Park, *Small*, 2015, **11**, 10–25.
- 5 G. Xing, N. Mathews, S. Sun, S. S. Lim, Y. M. Lam, M. Grätzel, S. Mhaisalkar and T. C. Sum, *Science*, 2013, **342**, 344–347.
- 6 S. D. Stranks, G. E. Eperon, G. Grancini, C. Menelaou, M. J. P. Alcocer, T. Leijtens, L. M. Herz, A. Petrozza and H. J. Snaith, *Science*, 2013, **342**, 341–344.
- 7 A. Kojima, K. Teshima, Y. Shirai and T. Miyasaka, *J. Am. Chem. Soc.*, 2009, **131**, 6050–6051.
- 8 http://www.nrel.gov/ncpv/images/efficiency_chart.jpg.
- 9 J. You, L. Meng, T.-B. Song, T.-F. Guo, Y. Yang, W.-H. Chang, Z. Hong, H. Chen, H. Zhou, Q. Chen, Y. Liu and N. De Marco, *Nat. Nanotechnol.*, 2016, **11**, 75–81.
- 10 T. Leijtens, G. E. Eperon, N. K. Noel, S. N. Habisreutinger, A. Petrozza and H. J. Snaith, *Adv. Energy Mater.*, 2015, **5**, 1500963.
- 11 N. H. Tiep, Z. Ku and H. J. Fan, *Adv. Energy Mater.*, 2016, **6**, 1501420.
- 12 Y. Rong, L. Liu, A. Mei, X. Li and H. Han, *Adv. Energy Mater.*, 2015, **5**, 1501066.
- 13 T. A. Berhe, W.-N. Su, C.-H. Chen, C.-J. Pan, J.-H. Cheng, H.-M. Chen, M.-C. Tsai, L.-Y. Chen, A. A. Dubale and B.-J. Hwang, *Energy Environ. Sci.*, 2016, **9**, 323–356.
- 14 B. R. Vincent, K. N. Robertson, T. S. Cameron and O. Knop, *Can. J. Chem.*, 1987, **65**, 1042–1046.
- 15 A. Wakamiya, M. Endo, T. Sasamori, N. Tokitoh, Y. Ogomi, S. Hayase and Y. Murata, *Chem. Lett.*, 2014, **43**, 711–713.
- 16 A. M. A. Leguy, Y. Hu, M. Campoy-Quiles, M. I. Alonso, O. J. Weber, P. Azarhoosh, M. van Schilfgaarde, M. T. Weller, T. Bein, J. Nelson, P. Docampo and P. R. F. Barnes, *Chem. Mater.*, 2015, **27**, 3397–3407.
- 17 J. A. Christians, P. A. Miranda Herrera and P. V. Kamat, *J. Am. Chem. Soc.*, 2015, **137**, 1530–1538.
- 18 J. Yang, B. D. Siempelkamp, D. Liu and T. L. Kelly, *ACS Nano*, 2015, **9**, 1955–1963.
- 19 H. Zhou, Q. Chen, G. Li, S. Luo, T.-b. Song, H.-S. Duan, Z. Hong, J. You, Y. Liu and Y. Yang, *Science*, 2014, **345**, 542–546.
- 20 J. You, Y. Yang, Z. Hong, T.-B. Song, L. Meng, Y. Liu, C. Jiang, H. Zhou, W.-H. Chang and G. Li, *Appl. Phys. Lett.*, 2014, **105**, 183902.
- 21 G. E. Eperon, V. M. Burlakov, P. Docampo, A. Goriely and H. J. Snaith, *Adv. Funct. Mater.*, 2014, **24**, 151–157.
- 22 B.-E. Cohen, S. Gamliel and L. Etgar, *APL Mater.*, 2014, **2**, 081502.
- 23 J. H. Noh, S. H. Im, J. H. Heo, T. N. Mandal and S. I. Seok, *Nano Lett.*, 2013, **13**, 1764–1769.
- 24 Z. Cheng and J. Lin, *CrystEngComm*, 2010, **12**, 2646–2662.
- 25 A. Dualeh, P. Gao, S. I. Seok, M. K. Nazeeruddin and M. Grätzel, *Chem. Mater.*, 2014, **26**, 6160–6164.

- 26 S. Aharon, A. Dymshits, A. Rotem and L. Etgar, *J. Mater. Chem. A*, 2015, **3**, 9171–9178.
- 27 R. K. Misra, S. Aharon, B. Li, D. Mogilyansky, I. Visoly-Fisher, L. Etgar and E. A. Katz, *J. Phys. Chem. Lett.*, 2015, **6**, 326–330.
- 28 T. Leijtens, E. T. Hoke, G. Grancini, D. J. Slotcavage, G. E. Eperon, J. M. Ball, M. De Bastiani, A. R. Bowring, N. Martino, K. Wojciechowski, M. D. McGehee, H. J. Snaith and A. Petrozza, *Adv. Energy Mater.*, 2015, **5**, 1500962.
- 29 Z. Xiao, Y. Yuan, Y. Shao, Q. Wang, Q. Dong, C. Bi, P. Sharma, A. Gruverman and J. Huang, *Nat. Mater.*, 2015, **14**, 193–198.
- 30 F. Hao, C. C. Stoumpos, D. H. Cao, R. P. H. Chang and M. G. Kanatzidis, *Nat. Photonics*, 2014, **8**, 489–494.
- 31 M. H. Kumar, S. Dharani, W. L. Leong, P. P. Boix, R. R. Prabhakar, T. Baikie, C. Shi, H. Ding, R. Ramesh, M. Asta, M. Graetzel, S. G. Mhaisalkar and N. Mathews, *Adv. Mater.*, 2014, **26**, 7122–7127.
- 32 N. K. Noel, S. D. Stranks, A. Abate, C. Wehrenfennig, S. Guarnera, A.-A. Haghighirad, A. Sadhanala, G. E. Eperon, S. K. Pathak, M. B. Johnston, A. Petrozza, L. M. Herz and H. J. Snaith, *Energy Environ. Sci.*, 2014, **7**, 3061–3068.
- 33 G. Niu, X. Guo and L. Wang, *J. Mater. Chem. A*, 2015, **3**, 8970–8980.
- 34 B. J. Foley, D. L. Marlowe, K. Sun, W. A. Saidi, L. Scudiero, M. C. Gupta and J. J. Choi, *Appl. Phys. Lett.*, 2015, **106**, 243904.
- 35 J. Yang, B. D. Siempelkamp, E. Mosconi, F. De Angelis and T. L. Kelly, *Chem. Mater.*, 2015, **27**, 4229–4236.
- 36 C. C. Stoumpos, C. D. Malliakas and M. G. Kanatzidis, *Inorg. Chem.*, 2013, **52**, 9019–9038.
- 37 J.-W. Lee, D.-J. Seol, A.-N. Cho and N.-G. Park, *Adv. Mater.*, 2014, **26**, 4991–4998.
- 38 E. T. Hoke, D. J. Slotcavage, E. R. Dohner, A. R. Bowring, H. I. Karunadasa and M. D. McGehee, *Chem. Sci.*, 2015, **6**, 613–617.
- 39 H.-S. Kim, C.-R. Lee, J.-H. Im, K.-B. Lee, T. Moehl, A. Marchioro, S.-J. Moon, R. Humphry-Baker, J.-H. Yum, J. E. Moser, M. Grätzel and N.-G. Park, *Sci. Rep.*, 2012, **2**, 591.
- 40 J. Burschka, N. Pellet, S.-J. Moon, R. Humphry-Baker, P. Gao, M. K. Nazeeruddin and M. Grätzel, *Nature*, 2013, **499**, 316–319.
- 41 J. M. Ball, M. M. Lee, A. Hey and H. J. Snaith, *Energy Environ. Sci.*, 2013, **6**, 1739–1743.
- 42 W. S. Yang, J. H. Noh, N. J. Jeon, Y. C. Kim, S. Ryu, J. Seo and S. I. Seok, *Science*, 2015, **348**, 1234–1237.
- 43 K. Wang, Y. Shi, B. Li, L. Zhao, W. Wang, X. Wang, X. Bai, S. Wang, C. Hao and T. Ma, *Adv. Mater.*, 2016, **28**, 1891–1897.
- 44 Q. Dong, Y. Shi, K. Wang, Y. Li, S. Wang, H. Zhang, Y. Xing, Y. Du, X. Bai and T. Ma, *J. Phys. Chem. C*, 2015, **119**, 10212–10217.
- 45 T. Leijtens, G. E. Eperon, S. Pathak, A. Abate, M. M. Lee and H. J. Snaith, *Nat. Commun.*, 2013, **4**, 4885.
- 46 S. K. Pathak, A. Abate, P. Ruckdeschel, B. Roose, K. C. Gödel, Y. Vaynzof, A. Santhala, S.-I. Watanabe, D. J. Hollman, N. Noel, A. Sepe, U. Wiesner, R. Friend, H. J. Snaith and U. Steiner, *Adv. Funct. Mater.*, 2014, **24**, 6046–6055.
- 47 M. A. Henderson, W. S. Epling, C. L. Perkins, C. H. F. Peden and U. Diebold, *J. Phys. Chem. B*, 1999, **103**, 5328–5337.
- 48 G. Lu, A. Linsebigler and J. T. Yates, *J. Chem. Phys.*, 1995, **102**, 4657–4662.
- 49 S. Ito, S. Tanaka, K. Manabe and H. Nishino, *J. Phys. Chem. C*, 2014, **118**, 16995–17000.
- 50 J. Yin, J. Cao, X. He, S. Yuan, S. Sun, J. Li, N. Zheng and L. Lin, *J. Mater. Chem. A*, 2015, **3**, 16860–16866.
- 51 F. Matsumoto, S. M. Vorpahl, J. Q. Banks, E. Sengupta and D. S. Ginger, *J. Phys. Chem. C*, 2015, **119**, 20810–20816.
- 52 P. Ganesan, K. Fu, P. Gao, I. Raabe, K. Schenk, R. Scopelliti, J. Luo, L. H. Wong, M. Grätzel and M. K. Nazeeruddin, *Energy Environ. Sci.*, 2015, **8**, 1986–1991.
- 53 Z. Hawash, L. K. Ono, S. R. Raga, M. V. Lee and Y. Qi, *Chem. Mater.*, 2015, **27**, 562–569.
- 54 M.-C. Jung and Y. Qi, *Org. Electron.*, 2016, **31**, 71–76.
- 55 M.-C. Jung, S. R. Raga, L. K. Ono and Y. Qi, *Sci. Rep.*, 2015, **5**, 9863.
- 56 L. K. Ono, P. Schulz, J. J. Endres, G. O. Nikiforov, Y. Kato, A. Kahn and Y. Qi, *J. Phys. Chem. Lett.*, 2014, **5**, 1374–1379.
- 57 S. Wang, W. Yuan and Y. S. Meng, *ACS Appl. Mater. Interfaces*, 2015, **7**, 24791–24798.
- 58 S. Guarnera, A. Abate, W. Zhang, J. M. Foster, G. Richardson, A. Petrozza and H. J. Snaith, *J. Phys. Chem. Lett.*, 2015, **6**, 432–437.
- 59 A. Guerrero, J. You, C. Aranda, Y. S. Kang, G. Garcia-Belmonte, H. Zhou, J. Bisquert and Y. Yang, *ACS Nano*, 2016, **10**, 218–224.
- 60 Y. Kato, L. K. Ono, M. V. Lee, S. Wang, S. R. Raga and Y. Qi, *Adv. Mater. Interfaces*, 2015, **2**, 1500195.
- 61 V. Verdingovas, L. Müller, M. S. Jellesen, F. B. Grummen and R. Ambat, *Corros. Sci.*, 2015, **97**, 161–171.
- 62 A. Davis, T. Tran and D. R. Young, *Hydrometallurgy*, 1993, **32**, 143–159.
- 63 S. N. Habisreutinger, T. Leijtens, G. E. Eperon, S. D. Stranks, R. J. Nicholas and H. J. Snaith, *Nano Lett.*, 2014, **14**, 5561–5568.
- 64 G. Niu, W. Li, F. Meng, L. Wang, H. Dong and Y. Qiu, *J. Mater. Chem. A*, 2014, **2**, 705–710.
- 65 J. Qiu, Y. Qiu, K. Yan, M. Zhong, C. Mu, H. Yan and S. Yang, *Nanoscale*, 2013, **5**, 3245–3248.
- 66 L. Hu, G. Shao, T. Jiang, D. Li, X. Lv, H. Wang, X. Liu, H. Song, J. Tang and H. Liu, *ACS Appl. Mater. Interfaces*, 2015, **7**, 25113–25120.
- 67 G. Divitini, S. Cacovich, F. Matteocci, L. Cinà, A. Di Carlo and C. Ducati, *Nat. Energy*, 2016, 15012.
- 68 B. Philippe, B.-W. Park, R. Lindblad, J. Oscarsson, S. Ahmadi, E. M. J. Johansson and H. Rensmo, *Chem. Mater.*, 2015, **27**, 1720–1731.
- 69 J. Bisquert, I. Mora-Sero and F. Fabregat-Santiago, *Chem-ElectroChem*, 2014, **1**, 289–296.

- 70 M. Bag, L. A. Renna, R. Y. Adhikari, S. Karak, F. Liu, P. M. Lahti, T. P. Russell, M. T. Tuominen and D. Venkataraman, *J. Am. Chem. Soc.*, 2015, **137**, 13130–13137.
- 71 H. Yu, F. Wang, F. Xie, W. Li, J. Chen and N. Zhao, *Adv. Funct. Mater.*, 2014, **24**, 7102–7108.
- 72 M. Grätzel, *Nat. Mater.*, 2014, **13**, 838–842.
- 73 J. A. Christians, J. S. Manser and P. V. Kamat, *J. Phys. Chem. Lett.*, 2015, **6**, 852–857.
- 74 A. Buin, R. Comin, J. Xu, A. H. Ip and E. H. Sargent, *Chem. Mater.*, 2015, **27**, 4405–4412.
- 75 W.-J. Yin, J.-H. Yang, J. Kang, Y. Yan and S.-H. Wei, *J. Mater. Chem. A*, 2015, **3**, 8926–8942.
- 76 F. De Angelis, *Acc. Chem. Res.*, 2014, **47**, 3349–3360.
- 77 X. Dong, X. Fang, M. Lv, B. Lin, S. Zhang, J. Ding and N. Yuan, *J. Mater. Chem. A*, 2015, **3**, 5360–5367.
- 78 E. Mosconi, J. M. Azpiroz and F. De Angelis, *Chem. Mater.*, 2015, **27**, 4885–4892.
- 79 L. Zhang and P. H. L. Sit, *J. Phys. Chem. C*, 2015, **119**, 22370–22378.
- 80 J. Haruyama, K. Sodeyama, L. Han and Y. Tateyama, *J. Phys. Chem. Lett.*, 2014, **5**, 2903–2909.
- 81 J. M. Frost, K. T. Butler, F. Brivio, C. H. Hendon, M. van Schilfhaarde and A. Walsh, *Nano Lett.*, 2014, **14**, 2584–2590.
- 82 C. Eames, J. M. Frost, P. R. F. Barnes, B. C. O'Regan, A. Walsh and M. S. Islam, *Nat. Commun.*, 2015, **6**, 7497.
- 83 J. Haruyama, K. Sodeyama, L. Han and Y. Tateyama, *J. Am. Chem. Soc.*, 2015, **137**, 10048–10051.
- 84 A. Mei, X. Li, L. Liu, Z. Ku, T. Liu, Y. Rong, M. Xu, M. Hu, J. Chen, Y. Yang, M. Grätzel and H. Han, *Science*, 2014, **345**, 295–298.
- 85 S. Yang, Y. Wang, P. Liu, Y.-B. Cheng, H. J. Zhao and H. G. Yang, *Nat. Energy*, 2016, **1**, 15016.
- 86 G. E. Eperon, S. D. Stranks, C. Menelaou, M. B. Johnston, L. M. Herz and H. J. Snaith, *Energy Environ. Sci.*, 2014, **7**, 982–988.
- 87 T. M. Koh, K. Fu, Y. Fang, S. Chen, T. C. Sum, N. Mathews, S. G. Mhaisalkar, P. P. Boix and T. Baikie, *J. Phys. Chem. C*, 2014, **118**, 16458–16462.
- 88 Y. Fu, H. Zhu, A. W. Schrader, D. Liang, Q. Ding, P. Joshi, L. Hwang, X. Y. Zhu and S. Jin, *Nano Lett.*, 2016, **16**, 1000–1008.
- 89 N. J. Jeon, J. H. Noh, W. S. Yang, Y. C. Kim, S. Ryu, J. Seo and S. I. Seok, *Nature*, 2015, **517**, 476–480.
- 90 A. Binek, F. C. Hanusch, P. Docampo and T. Bein, *J. Phys. Chem. Lett.*, 2015, **6**, 1249–1253.
- 91 C. Yi, J. Luo, S. Meloni, A. Boziki, N. Ashari-Astani, C. Gratzel, S. M. Zakeeruddin, U. Rothlisberger and M. Gratzel, *Energy Environ. Sci.*, 2016, **9**, 656–662.
- 92 Z. Li, M. Yang, J.-S. Park, S.-H. Wei, J. J. Berry and K. Zhu, *Chem. Mater.*, 2016, **28**, 284–292.
- 93 D. Cui, Z. Yang, D. Yang, X. Ren, Y. Liu, Q. Wei, H. Fan, J. Zeng and S. Liu, *J. Phys. Chem. C*, 2016, **120**, 42–47.
- 94 D. B. Mitzi, *J. Chem. Soc., Dalton Trans.*, 2001, 1–12.
- 95 I. C. Smith, E. T. Hoke, D. Solis-Ibarra, M. D. McGehee and H. I. Karunadasa, *Angew. Chem.*, 2014, **126**, 11414–11417.
- 96 L. Dou, A. B. Wong, Y. Yu, M. Lai, N. Kornienko, S. W. Eaton, A. Fu, C. G. Bischak, J. Ma, T. Ding, N. S. Ginsberg, L.-W. Wang, A. P. Alivisatos and P. Yang, *Science*, 2015, **349**, 1518–1521.
- 97 K. Yao, X. Wang, F. Li and L. Zhou, *Chem. Commun.*, 2015, **51**, 15430–15433.
- 98 K. Yao, X. Wang, Y.-x. Xu and F. Li, *Nano Energy*, 2015, **18**, 165–175.
- 99 G. E. Eperon, G. M. Paterno, R. J. Sutton, A. Zampetti, A. A. Haghighirad, F. Cacialli and H. J. Snaith, *J. Mater. Chem. A*, 2015, **3**, 19688–19695.
- 100 M. Kulbak, D. Cahen and G. Hodes, *J. Phys. Chem. Lett.*, 2015, **6**, 2452–2456.
- 101 M. Kulbak, S. Gupta, N. Kedem, I. Levine, T. Bendikov, G. Hodes and D. Cahen, *J. Phys. Chem. Lett.*, 2016, **7**, 167–172.
- 102 Z. Chen, J. J. Wang, Y. Ren, C. Yu and K. Shum, *Appl. Phys. Lett.*, 2012, **101**, 093901.
- 103 J. Xiao, J. Shi, H. Liu, Y. Xu, S. Lv, Y. Luo, D. Li, Q. Meng and Y. Li, *Adv. Energy Mater.*, 2015, **5**, 1401943.
- 104 Y. Guo, C. Liu, K. Inoue, K. Harano, H. Tanaka and E. Nakamura, *J. Mater. Chem. A*, 2014, **2**, 13827–13830.
- 105 S. Ameen, M. S. Akhtar, H.-K. Seo and H.-S. Shin, *Langmuir*, 2014, **30**, 12786–12794.
- 106 Y. Xiao, G. Han, Y. Chang, H. Zhou, M. Li and Y. Li, *J. Power Sources*, 2014, **267**, 1–8.
- 107 T. Swetha and S. P. Singh, *J. Mater. Chem. A*, 2015, **3**, 18329–18344.
- 108 N. J. Jeon, J. Lee, J. H. Noh, M. K. Nazeeruddin, M. Grätzel and S. I. Seok, *J. Am. Chem. Soc.*, 2013, **135**, 19087–19090.
- 109 P. Qin, S. Paek, M. I. Dar, N. Pellet, J. Ko, M. Grätzel and M. K. Nazeeruddin, *J. Am. Chem. Soc.*, 2014, **136**, 8516–8519.
- 110 H. Nishimura, N. Ishida, A. Shimazaki, A. Wakamiya, A. Saeki, L. T. Scott and Y. Murata, *J. Am. Chem. Soc.*, 2015, **137**, 15656–15659.
- 111 S. Kazim, F. J. Ramos, P. Gao, M. K. Nazeeruddin, M. Gratzel and S. Ahmad, *Energy Environ. Sci.*, 2015, **8**, 1816–1823.
- 112 L. Zheng, Y.-H. Chung, Y. Ma, L. Zhang, L. Xiao, Z. Chen, S. Wang, B. Qu and Q. Gong, *Chem. Commun.*, 2014, **50**, 11196–11199.
- 113 Y. Ma, Y.-H. Chung, L. Zheng, D. Zhang, X. Yu, L. Xiao, Z. Chen, S. Wang, B. Qu, Q. Gong and D. Zou, *ACS Appl. Mater. Interfaces*, 2015, **7**, 6406–6411.
- 114 H. Choi, J. W. Cho, M.-S. Kang and J. Ko, *Chem. Commun.*, 2015, **51**, 9305–9308.
- 115 A. Abate, S. Paek, F. Giordano, J.-P. Correa-Baena, M. Saliba, P. Gao, T. Matsui, J. Ko, S. M. Zakeeruddin, K. H. Dahmen, A. Hagfeldt, M. Gratzel and M. K. Nazeeruddin, *Energy Environ. Sci.*, 2015, **8**, 2946–2953.
- 116 P. Qin, S. Tanaka, S. Ito, N. Tetreault, K. Manabe, H. Nishino, M. K. Nazeeruddin and M. Grätzel, *Nat. Commun.*, 2014, **5**, 3834.
- 117 J. A. Christians, R. C. M. Fung and P. V. Kamat, *J. Am. Chem. Soc.*, 2014, **136**, 758–764.
- 118 G. A. Sepalage, S. Meyer, A. Pascoe, A. D. Scully, F. Huang, U. Bach, Y.-B. Cheng and L. Spiccia, *Adv. Funct. Mater.*, 2015, **25**, 5650–5661.

- 119 L. Hu, W. Wang, H. Liu, J. Peng, H. Cao, G. Shao, Z. Xia, W. Ma and J. Tang, *J. Mater. Chem. A*, 2015, **3**, 515–518.
- 120 L. Etgar, P. Gao, P. Qin, M. Graetzel and M. K. Nazeeruddin, *J. Mater. Chem. A*, 2014, **2**, 11586–11590.
- 121 X. Xu, Z. Liu, Z. Zuo, M. Zhang, Z. Zhao, Y. Shen, H. Zhou, Q. Chen, Y. Yang and M. Wang, *Nano Lett.*, 2015, **15**, 2402–2408.
- 122 J.-Y. Jeng, K.-C. Chen, T.-Y. Chiang, P.-Y. Lin, T.-D. Tsai, Y.-C. Chang, T.-F. Guo, P. Chen, T.-C. Wen and Y.-J. Hsu, *Adv. Mater.*, 2014, **26**, 4107–4113.
- 123 H. Zhang, J. Cheng, F. Lin, H. He, J. Mao, K. S. Wong, A. K. Y. Jen and W. C. H. Choy, *ACS Nano*, 2016, **10**, 1503–1511.
- 124 B. Abdollahi Nejjand, V. Ahmadi and H. R. Shahverdi, *ACS Appl. Mater. Interfaces*, 2015, **7**, 21807–21818.
- 125 J. H. Kim, P.-W. Liang, S. T. Williams, N. Cho, C.-C. Chueh, M. S. Glaz, D. S. Ginger and A. K. Y. Jen, *Adv. Mater.*, 2015, **27**, 695–701.
- 126 M. Lv, J. Zhu, Y. Huang, Y. Li, Z. Shao, Y. Xu and S. Dai, *ACS Appl. Mater. Interfaces*, 2015, **7**, 17482–17488.
- 127 Q. Wu, C. Xue, Y. Li, P. Zhou, W. Liu, J. Zhu, S. Dai, C. Zhu and S. Yang, *ACS Appl. Mater. Interfaces*, 2015, **7**, 28466–28473.
- 128 W. Chen, Y. Wu, Y. Yue, J. Liu, W. Zhang, X. Yang, H. Chen, E. Bi, I. Ashraful, M. Grätzel and L. Han, *Science*, 2015, **350**, 944–948.
- 129 S. N. Habisreutinger, T. Leijtens, G. E. Eperon, S. D. Stranks, R. J. Nicholas and H. J. Snaith, *J. Phys. Chem. Lett.*, 2014, **5**, 4207–4212.
- 130 K. Aitola, K. Sveinbjornsson, J.-P. Correa-Baena, A. Kaskela, A. Abate, Y. Tian, E. M. J. Johansson, M. Gratzel, E. I. Kauppinen, A. Hagfeldt and G. Boschloo, *Energy Environ. Sci.*, 2016, **9**, 461–466.
- 131 E. J. Juarez-Perez, M. Wüßler, F. Fabregat-Santiago, K. Lakus-Wollny, E. Mankel, T. Mayer, W. Jaegermann and I. Mora-Sero, *J. Phys. Chem. Lett.*, 2014, **5**, 680–685.
- 132 N. Adhikari, A. Dubey, D. Khatiwada, A. F. Mitul, Q. Wang, S. Venkatesan, A. Iefanova, J. Zai, X. Qian, M. Kumar and Q. Qiao, *ACS Appl. Mater. Interfaces*, 2015, **7**, 26445–26454.
- 133 A. Guerrero, S. Chambon, L. Hirsch and G. Garcia-Belmonte, *Adv. Funct. Mater.*, 2014, **24**, 6234–6240.
- 134 I. Hwang, M. Baek and K. Yong, *ACS Appl. Mater. Interfaces*, 2015, **7**, 27863–27870.
- 135 Y. Ogomi, A. Morita, S. Tsukamoto, T. Saitho, Q. Shen, T. Toyoda, K. Yoshino, S. S. Pandey, T. Ma and S. Hayase, *J. Phys. Chem. C*, 2014, **118**, 16651–16659.
- 136 K. Wang, Y. Shi, Q. Dong, Y. Li, S. Wang, X. Yu, M. Wu and T. Ma, *J. Phys. Chem. Lett.*, 2015, **6**, 755–759.
- 137 A. Bera, A. D. Sheikh, M. A. Haque, R. Bose, E. Alarousu, O. F. Mohammed and T. Wu, *ACS Appl. Mater. Interfaces*, 2015, **7**, 28404–28411.
- 138 J. H. Yun, I. Lee, T.-S. Kim, M. J. Ko, J. Y. Kim and H. J. Son, *J. Mater. Chem. A*, 2015, **3**, 22176–22182.
- 139 M. Kaltenbrunner, G. Adam, E. D. Glowacki, M. Drack, R. Schwodiauer, L. Leonat, D. H. Apaydin, H. Groiss, M. C. Scharber, M. S. White, N. S. Sariciftci and S. Bauer, *Nat. Mater.*, 2015, **14**, 1032–1039.
- 140 M. Batmunkh, C. J. Shearer, M. J. Biggs and J. G. Shapter, *J. Mater. Chem. A*, 2015, **3**, 9020–9031.
- 141 P. Joshi, X. Yu, M. Ropp, D. Galipeau, S. Bailey and Q. Qiao, *Energy Environ. Sci.*, 2008, **2**, 426–429.
- 142 P. Joshi, L. Zhang, D. Davoux, Z. Zhu, D. Galipeau, H. Fong and Q. Qiao, *Energy Environ. Sci.*, 2010, **3**, 1507–1510.
- 143 M. Wu, X. Lin, T. Wang, J. Qiu and T. Ma, *Energy Environ. Sci.*, 2011, **4**, 2308–2315.
- 144 H. Zhou, Y. Shi, Q. Dong, H. Zhang, Y. Xing, K. Wang, Y. Du and T. Ma, *J. Phys. Chem. Lett.*, 2014, **5**, 3241–3246.
- 145 H. Zhou, Y. Shi, K. Wang, Q. Dong, X. Bai, Y. Xing, Y. Du and T. Ma, *J. Phys. Chem. C*, 2015, **119**, 4600–4605.
- 146 Z. Ku, Y. Rong, M. Xu, T. Liu and H. Han, *Sci. Rep.*, 2013, **3**, 3132.
- 147 L. Zhang, T. Liu, L. Liu, M. Hu, Y. Yang, A. Mei and H. Han, *J. Mater. Chem. A*, 2015, **3**, 9165–9170.
- 148 Z. Wei, H. Chen, K. Yan and S. Yang, *Angew. Chem.*, 2014, **126**, 13455–13459.
- 149 Z. Li, S. A. Kulkarni, P. P. Boix, E. Shi, A. Cao, K. Fu, S. K. Batabyal, J. Zhang, Q. Xiong, L. H. Wong, N. Mathews and S. G. Mhaisalkar, *ACS Nano*, 2014, **8**, 6797–6804.
- 150 Z. Wei, H. Chen, K. Yan, X. Zheng and S. Yang, *J. Mater. Chem. A*, 2015, **3**, 24226–24231.
- 151 Y. Yang, J. Xiao, H. Wei, L. Zhu, D. Li, Y. Luo, H. Wu and Q. Meng, *RSC Adv.*, 2014, **4**, 52825–52830.
- 152 Z. Wei, K. Yan, H. Chen, Y. Yi, T. Zhang, X. Long, J. Li, L. Zhang, J. Wang and S. Yang, *Energy Environ. Sci.*, 2014, **7**, 3326–3333.
- 153 P. You, Z. Liu, Q. Tai, S. Liu and F. Yan, *Adv. Mater.*, 2015, **27**, 3632–3638.
- 154 K. Cao, Z. Zuo, J. Cui, Y. Shen, T. Moehl, S. M. Zakeeruddin, M. Grätzel and M. Wang, *Nano Energy*, 2015, **17**, 171–179.
- 155 X. Li, M. Tschumi, H. Han, S. S. Babkair, R. A. Alzubaydi, A. A. Ansari, S. S. Habib, M. K. Nazeeruddin, S. M. Zakeeruddin and M. Grätzel, *Energy Technol.*, 2015, **3**, 551–555.
- 156 Z. Wei, X. Zheng, H. Chen, X. Long, Z. Wang and S. Yang, *J. Mater. Chem. A*, 2015, **3**, 16430–16434.
- 157 Y. Luo, X. Chen, C. Zhang, J. Li, J. Shi, Z. Sun, Z. Wang and S. Huang, *RSC Adv.*, 2015, **5**, 56037–56044.
- 158 Z. Jiang, X. Chen, X. Lin, X. Jia, J. Wang, L. Pan, S. Huang, F. Zhu and Z. Sun, *Sol. Energy Mater. Sol. Cells*, 2016, **146**, 35–43.
- 159 X. Li, M. Ibrahim Dar, C. Yi, J. Luo, M. Tschumi, S. M. Zakeeruddin, M. K. Nazeeruddin, H. Han and M. Grätzel, *Nat. Chem.*, 2015, **7**, 703–711.
- 160 Y. Zhao, J. Wei, H. Li, Y. Yan, W. Zhou, D. Yu and Q. Zhao, *Nat. Commun.*, 2016, **7**, 10228.
- 161 M. Jørgensen, K. Norrman, S. A. Gevorgyan, T. Tromholt, B. Andreasen and F. C. Krebs, *Adv. Mater.*, 2012, **24**, 580–612.
- 162 M. Jørgensen, K. Norrman and F. C. Krebs, *Sol. Energy Mater. Sol. Cells*, 2008, **92**, 686–714.
- 163 I. Hwang, I. Jeong, J. Lee, M. J. Ko and K. Yong, *ACS Appl. Mater. Interfaces*, 2015, **7**, 17330–17336.

- 164 Y. Han, S. Meyer, Y. Dkhissi, K. Weber, J. M. Pringle, U. Bach, L. Spiccia and Y.-B. Cheng, *J. Mater. Chem. A*, 2015, **3**, 8139–8147.
- 165 F. Matteocci, S. Razza, F. Di Giacomo, S. Casaluci, G. Mincuzzi, T. M. Brown, A. D'Epifanio, S. Licoccia and A. Di Carlo, *Phys. Chem. Chem. Phys.*, 2014, **16**, 3918–3923.
- 166 I. S. Kim and A. B. F. Martinson, *J. Mater. Chem. A*, 2015, **3**, 20092–20096.
- 167 S. M. Kang, N. Ahn, J.-W. Lee, M. Choi and N.-G. Park, *J. Mater. Chem. A*, 2014, **2**, 20017–20021.
- 168 J. H. Heo, D. H. Song and S. H. Im, *Adv. Mater.*, 2014, **26**, 8179–8183.
- 169 T. Leijtens, G. E. Eperon, S. Pathak, A. Abate, M. M. Lee and H. J. Snaith, *Nat. Commun.*, 2013, **4**, 2885.
- 170 I. C. Smith, E. T. Hoke, D. Solis-Ibarra, M. D. McGehee and H. I. Karunadasa, *Angew. Chem., Int. Ed.*, 2014, **53**, 11232–11235.
- 171 L. Liu, A. Mei, T. Liu, P. Jiang, Y. Sheng, L. Zhang and H. Han, *J. Am. Chem. Soc.*, 2015, **137**, 1790–1793.
- 172 Z. Liu, M. Zhang, X. Xu, L. Bu, W. Zhang, W. Li, Z. Zhao, M. Wang, Y.-B. Cheng and H. He, *Dalton Trans.*, 2015, **44**, 3967–3973.
- 173 Z. Wei, H. Chen, K. Yan and S. Yang, *Angew. Chem., Int. Ed.*, 2014, **53**, 13239–13243.
- 174 Y. Rong, Z. Ku, A. Mei, T. Liu, M. Xu, S. Ko, X. Li and H. Han, *J. Phys. Chem. Lett.*, 2014, **5**, 2160–2164.
- 175 F. Zhang, X. Yang, H. Wang, M. Cheng, J. Zhao and L. Sun, *ACS Appl. Mater. Interfaces*, 2014, **6**, 16140–16146.